LOW PHASE NOISE OSCILLATOR DESIGN AND SIMULATION USING LARGE SIGNAL ANALYSIS AND LOW FREQUENCY FEEDBACK NETWORKS

A THESIS

SUBMITTED TO THE DEPARTMENT OF ELECTRICAL AND

ELECTRONICS ENGINEERING

AND THE GRADUATE SCHOOL OF ENGINEERING AND SCIENCE

OF BILKENT UNIVERSITY

IN PARTIAL FULFILLMENT OF THE REQUIREMENTS

FOR THE DEGREE OF

MASTER OF SCIENCE

By

Çağatay Ertürk Güngör

August, 2013

I certify that I have read this thesis and that in my opinion it is fully adequate, in scope and in quality, as a thesis for the degree of Master of Science.

Prof. Dr. Ekmel Özbay(Co-advisor)

I certify that I have read this thesis and that in my opinion it is fully adequate, in scope and in quality, as a thesis for the degree of Master of Science.

Dr. Tarık Reyhan(Co-advisor)

I certify that I have read this thesis and that in my opinion it is fully adequate, in scope and in quality, as a thesis for the degree of Master of Science.

Prof. Dr. Hayrettin Köymen

I certify that I have read this thesis and that in my opinion it is fully adequate, in scope and in quality, as a thesis for the degree of Master of Science.

Prof. Dr. Erdem Yazgan

Approved for the Graduate School of Engineering and Science:

Prof. Dr. Levent Onural
Director of the Graduate School

ABSTRACT

LOW PHASE NOISE OSCILLATOR DESIGN AND SIMULATION USING LARGE SIGNAL ANALYSIS AND LOW FREQUENCY FEEDBACK NETWORKS

Çağatay Ertürk Güngör
M.S. in Electrical and Electronics Engineering
Supervisors: Prof. Dr. Ekmel Özbay
Dr. Tarık Reyhan
August, 2013

Spectral purity of oscillators is of great importance in both commercial and military systems. Implementing communication, radar, and Electronic Warfare systems with increasingly higher frequencies, wider bandwidths, greater data rates, and more complex modulation schemes require low phase noise signal sources.

There are still discrepancies in the literature about phase noise in signal sources. Although analytical models accomplish to describe the phase noise of known signal sources accurately, a unifying and reproducible model or method that provides a priori information for the design of a low phase noise oscillator is still not established. Due to this lack of methodical approach, mostly empirical design practices that are known to produce good results are widely adopted. Proposed design method is similar.

Design and simulation of a low phase noise Dielectric Resonator Oscillator is studied. Noise sources in oscillators are briefly summarized. Phase noise models are compared. Dielectric resonators, which use small, disc-shaped ceramic materials that have high quality factors at microwave and millimeter-wave frequencies, are introduced with a concise theoretical coverage.

Effect of circuit configuration on phase noise is studied on two different FET devices. Common-gate configuration gave best simulation results for both transistors.

Parameters of coupling to the resonator are studied based on large signal analysis of the active device. The optimal parameters are described with supporting simulation results. Comparisons with suboptimal designs are provided, results indicate that optimization improves the phase noise on the order of tens of dBs.

Low frequency feedback method is investigated. Simulation results showed significant improvement in close-in phase noise when such networks are used. A large data set is obtained with input parameters of frequency, device, bias point, and feedback configuration; and optimality of such schemes are discussed based on it.

The methods for suppressing both close-in and away from the carrier phase noise are presented in the most generalized way, only to be reproduced for the intended device of operation.

Keywords: Low Phase Noise, Dielectric Resonator Oscillator, 1/f Noise, Low Frequency Feedback.

ÖZET

BÜYÜK SİNYAL ANALİZİ VE ALÇAK FREKANSLI GERİ BESLEME KULLANILARAK DÜŞÜK FAZ GÜRÜLTÜLÜ OSİLATÖR TASARIM VE SİMÜLASYONU

Çağatay Ertürk Güngör
Elektrik ve Elektronik Mühendisliği, Yüksek Lisans
Tez Yöneticileri: Prof. Dr. Ekmel Özbay
Dr. Tarık Reyhan
Ağustos, 2013

Sinyal üreteçlerinin spektral temizliği, ticari ve askeri elektronik sistemlerin başarımı üzerinde etkili bir faktördür. Gittikçe artan çalışma frekanslarında daha geniş bantlı, daha yüksek veri aktarım hızlarına sahip ve daha karmaşık modülasyon yöntemleri kullanan haberleşme, telekomünikasyon, radar ve Elektronik Harp sistemlerinin gerçeklenmesi; ancak düşük faz gürültülü sinyal kaynaklarının kullanılmasıyla mümkün olabilmektedir.

Sinyal kaynaklarının faz gürültüsüyle ilgili, literatürde henüz netleşmemiş bazı alanlar bulunmaktadır. Analitik modeller mevcut sinyal kaynaklarının faz gürültüsü özelliklerini isabetle hesaplayabilirken; düşük faz gürültülü sinyal üreteci tasarımında esas alınabilecek, genelleştirilebilir ve yinelenebilir bilgi sağlayan bir yöntem veya model önerilmemiştir. Dolayısıyla, iyi sonuç verdiği bilinen ve genellikle gözleme dayalı tasarım yöntemlerinin bu maksatla kullanımı yaygındır. Bu çalışmada da benzer bir yöntem izlenmiştir.

Düşük faz gürültülü bir Dielektrik Rezonatör Osilatörün tasarım ve simülasyon aşamaları sunulmuştur. Osilatörlerdeki gürültü kaynakları özetlenmiş, faz gürültüsü modelleri kıyaslanmıştır. Mikrodalga ve milimetredalga frekanslarında yüksek kalite faktörü sağlayan, disk şeklinde küçük seramik malzemeler olan dielektrik rezonatörler hakkında, kısa bir teorik analizi de kapsayan bilgi verilmiştir.

Devre topolojisinin faz gürültüsü üzerine etkisi, iki FET transistör üzerinde incelenmiş ve her iki transistör için ortak-kapı (common-gate) topolojisinin en

uygun faz gürültüsünü verdiği simülasyon sonuçlarıyla gözlemlenmiştir.

Kullanılan transistörlerin büyük sinyal analizi temel alınarak, rezonatör bağlaşım parametreleri incelenmiştir. En uygun bağlaşım parametreleri belirlenmiş ve destekleyici simülasyon sonuçları sunulmuştur. En iyi tasarım modeli, kötü tasarımlarla kıyaslanmış ve uygun parametrelerin faz gürültüsünü on dB'ler ölçeğinde iyileştirdiği tespit edilmiştir.

Düşük frekanslı geri besleme yöntemlerinin etkinliği araştırılmıştır. Simülasyon sonuçlarına göre bu tip yapıların kullanımıyla taşıyıcı frekansın yakınında bulunan bölgede faz gürültüsü performansı belirgin biçimde iyileşmiştir. Çalışma frekansı, kullanılan transistör, besleme gerilim ve akımları ve düşük frekanslı geri besleme topolojisi değişkenlerini içeren geniş bir veri kümesi elde edilmiş ve en uygun değer seçimleri tartışılmıştır.

Taşıyıcıya yakın ve uzak frekans bölgelerinin her ikisinde de faz gürültüsü başarımını iyileştiren ve yalnızca kullanılan transistöre bağlı olarak tekrarlanmak üzere genelleştirilmiş bir tasarım yöntemi, simülasyon sonuçlarıyla birlikte sunulmuştur.

Anahtar sözcükler: Faz Gürültüsü, Dielektrik Rezonatör Osilatör, 1/f Gürültüsü, Alçak Frekanslı Geri Besleme.

Contents

1 Introduction **1**

2 Background **3**

2.1 Noise Sources in Oscillators 3

2.1.1 Low Frequency Noise 3

2.1.2 Thermal Effects 9

2.1.3 Power Supply Noise 10

2.1.4 Tuning Varactor Noise 12

2.2 Phase Noise Models 13

2.2.1 Leeson Model 13

2.2.2 Lee-Hajimiri Model 15

2.2.3 Kurokawa Model 16

2.2.4 Everard Model 18

2.3 Dielectric Resonators 19

2.3.1 Historical Background of Dielectric Resonators 19

2.3.2 Theory of Operation 20

2.3.3 Quality Factor 23

2.3.4 Frequency and Phase Response of the Dielectric Resonator 28

3 Design Method 32

3.1 Previous Work 32

3.1.1 1/f Noise Reduction 32

3.2 Design Phases 35

3.2.1 Device Selection 35

3.2.2 Bias Point and Bias Networks 36

3.2.3 Circuit Configuration 37

3.2.4 Stability Analysis 38

3.2.5 Electromagnetic Simulations and EM/Circuit Co-Simulations 40

3.2.6 Resonator Simulation 41

3.2.7 Output Matching 43

3.2.8 Large Signal Analysis and Optimization 46

4 Results 50

4.1 Resonator Measurements 51

4.2 Comparison of Devices, Circuit Configurations, and Bias 53

4.3 Effect of Resonator Coupling on Phase Noise 54

4.4 Large Signal Optimization 55

4.5 Low Frequency Feedback Techniques 57

4.5.1 Output-to-Input Low Frequency Feedback 57

4.5.2 Complex Feedback Schemes 60

5 Conclusion **69**

A Feedback Configurations **77**

List of Figures

2.1 Random Telegraph Signal in time domain 9

2.2 Intersection of resonator and active device responses 16

2.3 Photograph of some Dielectric Resonators 20

2.4 Field distribution in $TE_{01\delta}$ mode 22

3.1 Device with feedback stub 39

3.2 Stability analysis of the device with feedback 40

3.3 A design example that uses EM component 41

3.4 Simulation results of the dielectric resonator coupled to microstrip 43

3.5 Output matching sweep simulation 45

3.6 Corresponding input impedances loci for swept output impedances 46

3.7 Tuning of transistor input reflection coefficient 47

3.8 Nyquist test results of the same tuning 48

3.9 Phase noise comparison of circuits with varying input reflection coefficients 49

4.1 Measured resonator frequency response and quality factor calculations 51

4.2 Measured resonator frequency response with top cover and quality factor calculations 52

4.3 Large signal analysis of the device with measured resonator response 53

4.4 Simulated phase noise vs. resonator insertion loss 55

4.5 Varying coupling simulation results 56

4.6 Comparison of the frequency responses of three alternative feedback filters 58

4.7 Harmonic Balance simulation results of the oscillator circuit with LPF feedback 59

4.8 Phase noise comparison of the oscillators with and without feedback network 60

4.9 Low Frequency Loops in a Common-Gate DRO Circuit 61

4.10 Frequency Response of the Feedback Low-Pass Filter 61

4.11 Frequency Response of the Feedback Band-Pass Filter 62

4.12 Effect of DC blocking the resonator at 9.15 GHz 66

4.13 Effect of DC blocking the resonator at 11.45 GHz 67

4.14 Maximum Phase Noise Improvement at 9.15 GHz 67

4.15 Maximum Phase Noise Improvement at 11.45 GHz 68

List of Tables

4.1 Phase Noise Performance Comparisons 54

4.2 Phase Noise Degradation Depending on the Intersection Angles . 57

4.3 Performance Comparison of Feedback Networks at 9.15 GHz . . . 63

4.4 Performance Comparison of Feedback Networks at 11.45 GHz . . 64

4.5 Performance Comparison of Feedback Networks at 11.45 GHz when DR is DC blocked 65

A.1 Feedback Networks Implemented 78

Chapter 1

Introduction

Spectral purity of oscillators is of great importance in both commercial and military systems. Implementing communication, radar, and Electronic Warfare systems with higher frequencies, wider bandwidths, greater data rates, and more complex modulation schemes require low phase noise signal sources.

Noise sources in oscillators are briefly introduced. Theoretical and experimental modeling of low frequency noise, which is the main contributor of close-in phase noise in oscillators is discussed, along with underlying physical mechanisms. Mathematical models of phase noise are compared. Dielectric resonators are introduced, and their behavior as a resonator is briefly studied.

Following the resonator analysis, design method for obtaining a low phase noise oscillator is presented. Low frequency feedback network method is shown to improve close-in phase noise, and large signal analysis based optimization method is shown to improve the phase noise away from the carrier frequency and to decrease the noise floor.

Measured frequency response data of the dielectric resonator is presented along with quality factor calculations. Data are shown to be consistent with ideal resonator model. Simulation results are obtained by importing the measured data

into RF/Electromagnetic co-simulation environment. Effect of shielding on resonator quality factor and resonant frequency tuning is illustrated. Finally the results and discussion of the extensive simulation data set is presented.

Chapter 2

Background

2.1 Noise Sources in Oscillators

2.1.1 Low Frequency Noise

Low frequency noise affects the phase noise performances of the amplifiers operating at high frequencies. Through an up-conversion process, low frequency noise could set the performance limits of microwave circuits like oscillators, multipliers, mixers and broadband amplifiers.

The current density j through any neutral n-doped semiconductor device can be written as $j = qnv$ where q is the electron charge, n is the majority carrier density and v is the majority carrier velocity. Fluctuations of these elements cause a resulting fluctuation of the current, which they constitute. Noisy behavior that are due to the fluctuations in q, n and v quantities are referred to as shot noise, number fluctuation noise and diffusion noise, respectively. Shot noise and diffusion noise are independent from frequency at usual frequencies and temperatures, i.e. they are white noise. Since the corpuscular nature and random motion of the involved carriers, they are irreducible under given bias and temperature conditions, thus forming the noise floor [1].

Number fluctuation noise has a different nature, however. Underlying mechanism is mainly trapping of the electrons at the defect centers, also referred to as generation recombination (G.R.) noise centers. Hence the noise amplitude is in proportion with the density of these trapping centers in the semiconductor. Considering the fact that such a generation recombination process has a time constant τ, which is observed to be usually below 1 ns at 300K, noise amplitude is inversely proportional to the frequency, at the frequencies beyond $2\pi\tau$. Therefore, this frequency dependent noise is dominated by the shot and diffusion noises at frequencies that exceed a certain value. This frequency value is called corner frequency and denoted as f_c [1]. Corner frequency can be considered as an indicator of the low frequency noise performance of a given device, and is incorporated in some phase noise models, which are discussed in this chapter.

2.1.1.1 Flicker Noise

Using an alternative noise classification, two noise types can be defined: additive and parametric. While thermal noise and shot noise are additive white noise, parametric noise term corresponds to both microscopic noise sources and environmental sources, which can be due to temperature fluctuation ($1/f^5$), power supply fluctuation (usually at 50-60 Hz) etc. Due to the fact that near-dc white noise does not contribute significantly to parametric noise in practice, and environmental fluctuations' contribution can be seen only at very low offset frequencies, flicker noise term is generally used ambiguously for the parametric noise term [2]. Contact noise term is also used synonymously in the literature for flicker noise, which was initially called as excess noise.

After its recognition by Johnson in 1925 [3], it was studied in thin films and carbon microphones. Further inspections revealed that noise with a spectrum scaling of the type $1/f^\gamma$, where γ is between 0.2 and 2, is present in a wide range of physical phenomena, including examples like the rate of radioactive decay, the flow rate of sand in an hourglass, the flux of cars on an expressway, the frequency of sunspots, the light output of quasars, the flow rate of the Nile over the last 2000 years, the water current velocity fluctuations at a depth of 3100 meters in

the Pacific ocean, in the loudness and pitch fluctuations of classical music etc. It has also been found below $10^{-8}Hz$ in the angular velocity of the earth's rotation, and below $10^{-4}Hz$ Hz in the relativistic neutron flux in the terrestrial atmosphere [2, 4, 1]. In general, a criterion developed in [4] to decide if an arbitrary system governed by a given system of differential equations will exhibit 1/f noise.

Spectral analysis for varying γ levels is provided in [5]. Although being extensively studied for many years, physical origin of 1/f noise in amplifiers has not been clearly understood and defined [6].

When modeling flicker noise of a given device, assuming that the noise would be of $1/f$ type with a rather straightforward approach, could lead to erroneous results. Considering the fact that γ coefficient in $1/f^{\gamma}$ is frequency dependent and varies in the range of 0.5 to 2, the necessity for the careful assessment of the proper value becomes obvious [1].

Physical parameters of semiconductors that describe the flicker noise behavior, like density and distribution of the generation and recombination centers, do not only differ from one device to another, but also depend on the biasing conditions. Therefore exact prediction of flicker noise performance is never available [1].

Models are used since unifying and satisfactory theory does not exist for flicker noise [1, 2]. In the following, two widely used flicker noise models are explained along with empirical modeling approaches.

2.1.1.1.1 McWhorter Model Electrons in the conduction band can get trapped into or move from the localized defect centers at the interface, according to this model. The trapped electrons at the interface can also get captured or emitted with defect centers in the oxide that have the same energy through the tunneling mechanism.

This model defines four movement directions for the electrons in the conduction band, a trapping into (process a) or moving away (process b) from defect centers; or a capture into (process c) or emitting from (process d) the oxide layer

[6].

The electron continuity, the interface trap continuity, and oxide trap continuity are then defined by integrating the volume density of oxide traps with energy level E, and the sheet density of the interface traps that can exchange electrons with the oxide traps with the same energy level E, over the interface area and control volume. Other parameters are the Shockley density, which is equal to the electron density when the electron quasi-Fermi energy is equal to E, and the tunneling coefficient with the unit of $cm^2\,sec^{-1}$ [6].

2.1.1.1.2 Hooge Model This model, also known as Hooge's Empirical Relation, is expressed with the following equation [6]:

$$S_{I,I} = \frac{\alpha_H}{f}\frac{I^2}{N}$$

where α_H denotes the Hooge's parameter. A local colored, i.e., frequency dependent noise source ζ_n is superimposed in the current density. The continuity equation for the conduction band electron is then [6]:

$$\nabla\left(J_n + \zeta_n\right) = q\frac{\partial n}{\partial t}$$

where n is the electron volume density in the conduction band at the interface.

Transfer function for Hooge's noise source is the gradient of Green's function for the electron continuity equation [6].

2.1.1.1.3 Empirical Models In addition to these models, use of an empirical coefficient in order to assess the flicker noise performance of an amplifier is suggested in [2].

Frequency independent part of the phase noise spectrum, i.e. white phase noise of the amplifier is equal to the power spectral density, which is the average

square phase noise per unit bandwidth. It is thus

$$b_0 = \frac{NB}{P_0} = \frac{FkT}{P_0}$$

where NB is the noise power in the bandwidth B, F is the noise figure of the amplifier, k is Boltzmann constant, T is the temperature, and P_0 is the carrier power.

In order to add the noise sidebands that are observed around any nonzero carrier to this simple PSD calculation; phase noise is described as the combination of the white and flicker noise [2]:

$$S(f) = b_0 + b_{-1}f^{-1} \quad (b_{-1} \approx constant\, vs.\, V_i)$$

where V_i is voltage level of the signal at the amplifier input and the coefficient b_{-1} is an experimental parameter for a specific amplifier, which is insensitive to input signal level.

In this approach, corner frequency is the frequency at which the white noise equals the flicker noise

$$f_c = \frac{b_{-1}}{b_0} = \frac{b_{-1}}{FkT_0}P_0$$

Noise floor decreases and corner frequency increases as the carrier power increases.

If the phase noise floor measurement is specified without the amplifier's input power, the information is incomplete. Specification of the flicker noise in terms of corner frequency is similarly insufficient due to this power dependence. Use of such experimental coefficient has the advantage of eliminating the power ambiguity.

Modeling based on such experimental parameter relaxes the need for complicated flicker noise models at the cost of experimenting. This trade-off could be viable depending on the application, since the nonlinearity level is high to model accurately. Even the devices from the same wafer usually exhibit dispersed low frequency noise characteristics due to the inhomogeneities [1], and the models lose their validity is small-size devices.

Such an empirical model is proposed in [7] for bipolar transistors. Equivalent noise generators are added to noiseless device model in this approach. Measurements are done in 100 Hz 100 kHz bandwidth, with bias varying. It is reported that in many practical applications, some EN generators dominate the stochastic process and others can be neglected. Hence the matrices that constitute the core of the model become strongly sparse.

There also have been efforts to model the up-conversion of the flicker noise. A model that is developed for linear HBT amplifiers, predicts 1/f PM and AM noise which is due to the up-conversion of 1/f baseband current noise. Observing the tuning effects of circuit parameters over phase noise is also possible using such a model [8].

As the flicker noise is not the major concern that determines the device size, it's always in a trend of being scaled down in favor of some other crucial aspects like higher overall performance and lower power consumption. This miniaturization is reported to transform the low frequency noise spectrum from a usual 1/f shape to a more Lorentzian-like one, with a larger device-to-device variation. Therefore the models introduced beforehand should not be assumed valid for the scaled devices [9].

A statistical model for small MOSFETs, which defines the area dependence of flicker noise mean and variation, is proposed in [9]. In this work, it's also been observed that flicker noise variability shows a log normal distribution.

Noncompliance of the flicker noise models with small size devices has a straight-forward physical explanation: Each electron trap contributes a Lorentzian noise, resulting in a 1/f noise spectrum in large devices with many

traps, and a less uniform, more Lorentzian like noise spectrum in small devices, which have only a few traps. Device-to-device variation is also justified implicitly in this way, considering the random distribution process of the traps [9].

Fluctuations due to electron traps show Random Telegraph Signal type behavior in time domain, as shown in Fig.2.1. In frequency domain, they are expressed as Lorentzian noise. Power spectrum and auto-correlation functions of the single and multi-Lorentzian noise combinations can be found in [5].

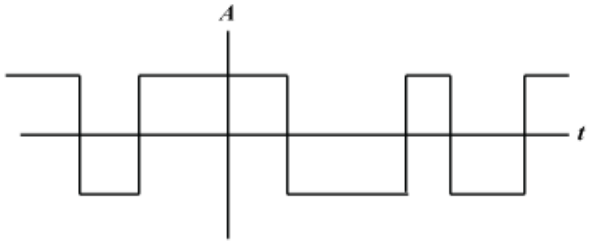

Figure 2.1: Random Telegraph Signal in time domain

2.1.2 Thermal Effects

It is reported that temperature fluctuations reflect to noise with a spectrum proportional to $1/f^5$. Better thermal shielding and higher thermal inertia lower the $1/f^5$ region in frequency dimension. However the effect of environmental temperature fluctuations is not clearly known to infiltrate the heat propagation within the circuit [2].

Cooling the oscillator circuit down to cryogenic temperatures is a method for noise reduction, which is primarily adopted for lowering the noise floor. Such a design shows that the sensitivity of flicker noise to gate and varactor bias is insignificantly low at 77 K, and the flicker noise level itself is slightly reduced [10].

2.1.3 Power Supply Noise

There's not much work in the literature on the effects of power supply noise over phase noise in oscillators.

Fluctuations on DC supply voltage modulate the amplitude and phase of the amplifier's output. This modulation effect is referred to as pushing, modulation noise or AM-to-PM conversion in the literature [11, 12, 13].

Voltage and current dependent capacitances of the transistor cause this unwanted modulation. To model this effect, it is suggested to assume the fixed tuning capacitor of the oscillator is a semiconductor junction which is reverse biased [11]. Using this approach, supply voltage noise is translated into the slight modulation effect of a hypothetical tuning diode. Using Nyquist's equation:

$$V_n = \sqrt{4kT_0R_{eq}\delta f}$$

where R_{eq} is the equivalent noise resistor, and δf is the bandwidth, determines an open noise voltage across the tuning diode [11].

Noise voltage V_n, generated by the tuning diode, is multiplied with amplifier gain. The rms frequency deviation in a 1 Hz bandwidth is calculated by [11]:

$$\delta f_{rms} = K_0 V_n$$

The equivalent peak phase deviation in the same bandwidth is:

$$\Theta_d = \frac{K_0\sqrt{2}}{f_m} V_n$$

Expressing in terms of the SSB signal to noise ratio:

$$L\left(f_m\right) = 20\log\frac{\Theta_c}{2}$$

It should be noted that this noise is regardless of the Q. Addition of this varactor tuning effect to the Leeson model is discussed in Phase Noise Models section.

Although the effect is mentioned in many sources and explanations with mathematical descriptions are available in some of them, a novel reduction technique is not available.

Adjusting the oscillator parameters to reduce the sensitivity of the operation frequency to the supply voltage is the ultimate trivial solution. Both fine tuning of the bias circuitry through trial-and-error, and isolating the oscillator from power supply using voltage regulators are under coverage of this parameter adjustment definition [12, 11].

DC output voltage of such devices with poor performance may contain broadband noise components that last for a time on the order of minutes, thus degrading the oscillator's SSB phase noise several decibels. Therefore it is advised in the literature that voltage regulators should be used carefully for noise suppression and devices with unspecified, unpredictable and erratic noise performances should be avoided [14]. Given the small current consumption of a typical oscillator, a simple series resistance and shunt capacitance network is suggested as solution. Filtering of buffer amplifiers could be done on a separate line due to their looser filtering requirements [12, 15].

Phase noise contribution of different voltage regulators to the oscillator with a feed-forward amplifier configuration given in [13] sets an example of the need for careful component choice. It is reported that SSB phase noise level is improved by approximately 13-14 dB by replacing the initial voltage regulators with ones that have lower noise floors.

In order to accurately assess the phase noise performance of an oscillator without power supply noise effects, it is advised to use chemical batteries since they are known to have very low 1/f noise levels [15].

2.1.4 Tuning Varactor Noise

In VCO circuits, varactors are used in order to provide a tunable capacitance. Resonator circuit's resonance frequency, and hence the final oscillation frequency is set as desired by tuning the varactor voltage. The magnitude of the non-linearity in the capacitance versus voltage curve of the varactor, translates into the phase noise of the oscillator. Varactor's Q factor and series resistance affect the resonator Q, therefore it could be the determining element on the oscillator performance. [11, 14].

It is advised to maximize the resonator Q; and simultaneously minimize the coupling for maximum loaded Q and the varactor series resistance if any [1].

If the oscillator uses a tuning varactor, it must be biased to as high a voltage as possible to reduce its effective nonlinear capacitance. On the capacitance versus voltage curve, large slope of capacitance at low bias is claimed to be the source of varactor-caused instabilities [14].

Tuning diodes are two types: abrupt and hyperabrupt. Abrupt junctions are linearly doped PN junctions. Their typical capacitance change is 4:1 or less over the specified range or reverse bias. The hyperabrupt junctions are nonlinearly doped and they have higher value of capacitance change versus reverse bias, on the order of 10:1 or more [11]. Hyperabrupt diodes have higher series resistance and lower Q [11]. Thus abrupt diodes have better phase noise performance.

Tuning diodes manufactured in GaAs process have lower capacitance for the same resistance due to the higher electron mobility than the Si process. Thus their Q values are greater than their silicon counterparts. However the silicon diodes have the advantage of lower flicker noise [11].

In order to limit the effects of varactor noise and nonlinearity, control schemes for combination of fixed and variable capacitances could be implemented [16].

In [17], frequency is tuned to discrete values via a switched capacitor array and the varactor is used for only the tuning between the adjacent frequencies, instead

of the full frequency range. Hence the performance degradation that would be observed otherwise due to wide capacitance range is limited to a degree.

Due to inherent limitations of the conventional semiconductor varactors, alternative structures are also being investigated by researchers. Although being primarily proposed for wideband tuning purposes, Tunable Active Inductor structure based on gyrator achieves good phase noise performance due to its relatively higher quality factor, which is reported to be greater than 500 at 9 GHz [16].

Performance of an oscillator with Barium Strontium Titanate (BST) varactor is investigated in [18]. Results showed that the varactor Q is lower than that of a junction varactor. However the capacitance versus voltage curve is much linear, which resulted in slightly better phase noise performance.

MEMS based varactors are also being studied, however a structure with high quality factor and sufficiently broad tuning range is not reported yet for replacing the junction varactors in high frequency VCOs.

2.2 Phase Noise Models

2.2.1 Leeson Model

Single-sideband phase noise of an oscillator according to Leeson model is given by [19]:

$$L(f_m) = 10\log\left[\frac{1}{2}\left(\left(\frac{\omega_0}{2Q_L f_m}\right)^2 + 1\right)\left(\frac{\omega_c}{\omega_m} + 1\right)\left(\frac{FkT_0}{P_{sav}}\right)\right]$$

where ω_m is frequency offset, ω_0 is center frequency, ω_c is flicker corner frequency, Q_L is loaded Q of the resonator, P_{sav} is the average power at oscillator output, and F is noise factor.

Model is expanded in [11] by expressing the loaded quality factor in terms

of unloaded quality factor, reactive energy stored in the resonator, and total dissipated power as

$$L(f_m) = \frac{1}{2}\left[1 + \frac{\omega_0^2}{4\omega_m^2}\left(\frac{P_{in}}{\omega_0 W_e} + \frac{1}{Q_0} + \frac{P_{sig}}{\omega_0 W_e}\right)^2\right]\left(1 + \frac{\omega_c}{\omega_m}\right)\frac{FkT_0}{P_{sav}}$$

where W_e is the reactive energy stored in resonator, Q_0 is unloaded Q of the resonator, P_{in} is the input power, and P_{sig} is the signal power.

As could be seen in the given equation, the model calculates the effects of resonator quality factor, up-converted flicker FM noise, thermal FM noise, the flicker phase noise and the thermal noise floor. Some necessary inputs to the equation such as the loaded Q, noise factor of the amplifier under large-signal conditions, the RF output power are unknown, which is drawback of this model [11, 20].

The model also does not include the power supply noise contributions. Incorporating the hypothetical tuning diode contribution described in Power Supply Noise subsection gives the following noise model [11]:

$$L(f_m) = 10\log\left[\left(1 + \frac{\omega_0^2}{(2\omega_m Q_L)^2}\right)\left(1 + \frac{\omega_c}{\omega_m}\right)\frac{FkT_0}{2P_{sav}} + \frac{2kT_0RK_0^2}{\omega_m^2}\right]$$

where R is equivalent noise resistance of the tuning diode, typically between 50 ohm-100 kohm and K_0 is oscillator voltage gain [11].

The author of [21] claims that he had done the exact same analysis in 1964, that it was used as a design guide in a series of oscillators which were widely used in USA and UK, and was not published for commercial reasons. Similar analysis and comments are provided in [21] with some notational differences.

2.2.2 Lee-Hajimiri Model

Lee-Hajimiri noise model is built upon an approach that investigates the time-varying properties of the oscillator's waveform. Phase noise analysis is done according to the effect of noise impulse on this periodic signal [22, 11, 20].

According to their theory, a noise impulse injection to a tuned circuit causes both amplitude and phase modulation with two extremities: injection at the peak of the signal causes maximum amplitude modulation with no effect on phase, and injection at the zero crossing of the signal causes maximum phase modulation with no effect on amplitude. Therefore minimal phase noise is obtained if the noise impulses coincide with the peaks of the oscillation signal [22, 11, 20].

Impulse Sensitivity Function (ISF) is introduced, which has its maximum value near the zero crossing of the oscillation signal. It indicates the sensitivity of moments to phase noise in a given oscillation cycle. Operating the oscillator under the guidance of this ISF, i.e., switching the oscillator on during short and less noise-sensitive time windows that are pointed out by ISF, results in a low phase noise oscillator [20]. Mathematical expression of the single-sideband phase noise is

$$L(f_m) = \begin{cases} 10\log\left[\frac{C_0^2}{q_{max}^2} * \frac{i_n^2\Delta f}{8f_m^2} * \frac{\omega_{1/f}}{f_m}\right] & : \frac{1}{f_3}\ region \\ 10\log\left[10\log\left(\frac{\Gamma_{rms}^2}{q_{max}^2} * \frac{i_n^2\Delta f}{4f_m^2}\right)\right] & : \frac{1}{f_2}\ region \end{cases}$$

where $i_n^2\Delta f$ is noise PSD, Δf is noise bandwidth, $\Gamma(x)$ is ISF, Γ_{rms}^2 is RMS value of $\Gamma(x)$, C_n is Fourier series coefficient, C_0 is 0^{th} order of the ISF, f_m is frequency offset from the carrier, $\omega_{1/f}$ is corner frequency and q_{max} is maximum charge stored across the resonator's capacitor.

Being built from a theoretical origin, following implementation issues are associated with this approach [11, 20, 23]: ISF is dependent on the oscillator topology and has a tedious calculation process. Conversion of the flicker noise is rather ambiguous. The ultimate phase noise equation is not expressed in terms of circuit parameters, thus the model does not provide any design guidance, ruling out any

chance for optimization of phase noise or power output performances.

For a given topology with an available data set the model is reported to give good results, though [11]. In a similar way with Leeson model, lack of prior information about the loaded Q, actual noise performance of the active device and the output power degrades the model's predictions. It's also noted that some of the published oscillators by Lee and Hajimiri could be optimized through the optimizer of a commercial harmonic balance program, with significant improvements on phase noise performance [11].

2.2.3 Kurokawa Model

For negative resistance and negative conductance oscillators, Kurokawa model describes conditions for both oscillation and optimal phase noise performance.

Fig.2.2 illustrates the resonator reflection coefficient, and active device reflection coefficient on complex plane. According to Kurokawa condition, the intersection angle between these two trajectories should be between 0 and 180 ° for the oscillation. In addition, phase noise is minimized if the trajectories are perpendicular [14, 24].

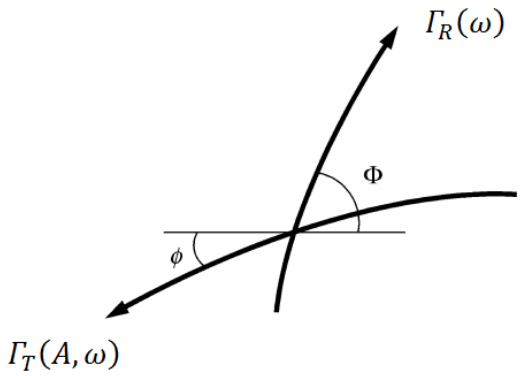

Figure 2.2: Intersection of resonator and active device responses

Nonlinear phase noise according to Kurokawa model is expressed as [25, 24]

$$S_\phi(f_m) = S_{\Delta\phi}(f_m)\left(\frac{f_0}{2Q_L f_m}\right)^2\left[1+\frac{q^2}{p^2+\left(\frac{2Q_L f_m}{f_0}\right)^2}\right]$$

where

$$S_{\Delta\phi}(f_m) = \frac{S_N}{P_L}\left(1+\frac{f_c}{f_m}\right)$$

$$p = \frac{A_0}{2Q_L\left(Re\{Y_S\}\right)^2}\left(\frac{\partial Re\{Y_A\}}{\partial A}\frac{\partial Im\{Y_S\}}{\partial f} - \frac{\partial Im\{Y_A\}}{\partial A}\frac{\partial Re\{Y_S\}}{\partial f}\right)$$

$$q = \frac{A_0}{2Q_L\left(Re\{Y_S\}\right)^2}\left(\frac{\partial Re\{Y_A\}}{\partial A}\frac{\partial Re\{Y_S\}}{\partial f} + \frac{\partial Im\{Y_A\}}{\partial A}\frac{\partial Im\{Y_S\}}{\partial f}\right)$$

where $S_{\Delta\phi}(f_m)$ is noise power spectral density normalized to the load power, which is denoted as P_L. S_N is a constant that is specific to a given transistor and defines the wideband noise characteristic of it. Y_A and Y_S denote the admittances of active circuit and resonator, respectively [26, 24].

The parameter p is a function of the stability conditions, and it also characterizes the start-up time of the oscillation. The parameter q illustrates the dependence of the oscillation frequency on the oscillation amplitude in a large signal mode of operation. Implications of the equations are as follows: As the parameter p becomes close to zero, noise increases. The region at which p is close to zero is also close to the boundary of the stable region. In addition, increase in q parameter degrades phase noise. Considering that this parameter describes the reflection of amplitude fluctuations on phase instability, the optimum defined as orthogonality between amplitude and phase behavior is quantitatively justified [24].

An extended version of Kurokawa approach which includes low frequency noise in GaAs MESFETs is expressed as [27]:

$$L(fb) = \frac{1}{2}\left(\frac{e_g(b)}{\omega_b}\frac{\partial\omega_c}{\partial V_{gs}}\right)^2$$

where $\frac{\partial\omega_c}{\partial V_{gs}}$ is the sensitivity of the carrier frequency with respect to the gate bias and corresponds to the pushing factor. Phase noise is approximated by a single noise voltage generator, denoted as $e_g(b)$, that is connected in series with the gate. Obviously this sensitivity is to be minimized. This could be achieved either by using a large Q resonator or by minimizing the sensitivity $\frac{\partial\Gamma_T}{\partial V_{gs}}$, where Γ_T is the active device large signal gate terminal reflection coefficient.

In a generalized approach, for devices with several voltage and current noise generators like bipolar transistor, a set of large signal sensitivities should be obtained and treated with a full nonlinear analysis [1].

2.2.4 Everard Model

A phase noise model that describes the spectrum in terms of the ratio of the loaded Q to unloaded Q is introduced by Everard [23].

Noise relation is described in a parametric way, depending on the power definition of the system. If the power is defined as total RF feedback power, which is the power in the oscillating system excluding the losses in the amplifier, it is denoted as P_{RF}. It is limited by the maximum voltage swing at the output of the amplifier. If the power in the oscillator is defined as the power available at the output of the amplifier, it is denoted as P_{AVO} [23].

Noise model is then

$$L(f_m) = A\frac{FkT}{8Q_0^2\left(\frac{Q_L}{Q_0}\right)^2\left(1-\frac{Q_L}{Q_0}\right)^N P}\left(\frac{f_0}{\Delta f}\right)^2$$

where $N = 1$ and $A = 2$ if the power definition is P_{RF}; while $N = 2$ and $A = 1$ if the power definition is P_{AVO}.

White phase noise portion of the spectrum is not included in given relation. It is seen that higher feedback power, P_{RF}, results in a larger ratio. For a given loaded Q and amplifier noise figure, sideband noise remains constant.

Phase noise optimization criteria of this model predicts a ratio of $\frac{Q_L}{Q_0}$ that is equal to $\frac{2}{3}$ and $\frac{1}{2}$ for P_{RF} and P_{AVO} power definitions, respectively [23, 13]. In the following chapter, optimality of these values are investigated and results are presented.

2.3 Dielectric Resonators

2.3.1 Historical Background of Dielectric Resonators

Resonators are fundamental elements of oscillators and filters. Their quality factor determines the performance of these circuits. Dielectric resonator is a low loss, temperature stable, small size resonator option for fixed frequency oscillators or narrow-band VCOs. They function as waveguide filters and resonant cavities, except that they are very small, stable and lightweight [28, 29].

A photograph of some resonators are given in Fig.2.3. Approximate resonance frequencies of the resonators in the Fig.2.3 are 6.15 GHz, 9.15 GHz, 11.60 GHz and 24 GHz; decreasing as the dimensions increase. The smaller cylindrical structures that are attached under two of the resonators are spacers. They are implemented primarily for isolating resonator boundary from the coupling microstrip to increase the resonator quality factor, which will be explained further in this chapter [29].

Guided electromagnetic wave propagation in dielectric media was subject to widespread attention in the early days of microwaves. Dielectric resonator term was first introduced in 1939 by R.D. Richtmyer of Stanford University, who showed that unmetalized dielectric objects like spheres and toroids can function as microwave resonators [30]. Inspiration of this theoretical work did not manifest itself for about 25 years. Modes and resonator design was analyzed in early

Figure 2.3: Photograph of some Dielectric Resonators

60's. However, poor temperature stability prohibited the practical use of high dielectric materials in microwave frequencies at the time [28].

Raytheon developed the first temperature stable, low loss ceramic dielectric resonators from Barium Tetratitanate in the early 70's. A modification that enhances the performance by Bell Labs followed that breakthrough [28]. Production of $(Zr - Sn)TiO_4$ ceramics by Murata in late 70's made these devices commercially available. Temperature coefficient between +10 and $12\,ppm/\,^{\circ}\mathrm{C}$ was possible by employing adjustable chemical compositions. Thereafter the theoretical work and utilization of dielectric resonators expanded rapidly [28].

Dimensions of the dielectric resonators get smaller as the desired resonant frequency increases. At very high millimeter wave frequencies, resonator becomes too small to be effectively used. Therefore, much larger resonators with whispering gallery modes are preferred, which were first observed by Rayleigh in a study of acoustic waves [28].

2.3.2 Theory of Operation

Dielectric resonator is coupled to microwave circuitry via microstrips or coupling loops.

Resonator is placed near the microstrip line on the substrate, usually within an enclosed cavity. The shielding conditions affect the resonant frequency and

the Q factor of the resonator [29].

A microwave cavity's resonance at a certain frequency is originated from the internal reflections of electromagnetic waves at the boundary that is between metal wall and air or vacuum that fills the cavity. Metal walls are electrical short due to their high conductivity. Inside the cavity enclosed with metal walls, reflections create a standing wave form with a specific electromagnetic field distribution, which is called a mode.

Common mode definitions are TE (Transverse Electric), TM (Transverse Magnetic) and TEM (Transverse Electromagnetic; also in some sources referred to as HEM, Hybrid Electromagnetic) modes. Indices show the number of field distribution variations along the corresponding coordinate. A TE_{113} mode means that there is only one distribution along x and y coordinates while three variations exist along z coordinate, for example.

Standard nomenclature for cavity modes describes the electromagnetic distribution of each possible mode that could be excited within a dielectric.

The magnetic wall concept - on which the normal component of the electric field and tangential component of the magnetic field vanish at the boundary - can be used to explain the behavior of dielectric resonator. For the sake of simplification of analytical calculations, it can be assumed that material with high dielectric constant/air boundary is an open circuit. However, the field distribution and resonant frequencies that are calculated under this assumption do not match the actual values, since the leaking EM field is ignored. In reality, a part of the EM field leaks out of the resonator body and decays exponentially through the outward direction. This leakage is inversely proportional to the dielectric constant of the material, as it might be guessed. In order to describe the leakage ratio, δ symbol is used as a mode subscript. δ is always smaller than unity and approaches one as the greater part of the EM field is conserved within the resonator [28].

In cavities, boundaries are short; therefore no leakage is of concern. That makes the solution of the electromagnetic field problem and calculation of modes for various cavity shapes easier than dielectric resonator [28].

Although the dielectric resonator has the simplest geometric form, finding an exact solution to the Maxwell equations is more difficult than for hollow cavities. Computations are done numerically, thus. A simple approximation for the resonant frequency is given by [29]:

$$f = \frac{8.5}{D\sqrt{\epsilon_r}} \left(\frac{D}{L} + 6.9 \right)$$

where f is the resonant frequency (in GHz), ϵ_r is the relative dielectric constant of the material, D and L are diameter and length of the resonator (in millimeters), respectively.

Results of this approximation is accurate with about 2 percent deviation [29], if

$$1 < \frac{D}{L} < 4 \; and \; 30 < \epsilon_r < 50$$

Calculation of the effects of more parameters, such as dielectric spacers, tuning plates and screws and substrate, requires more advanced models.

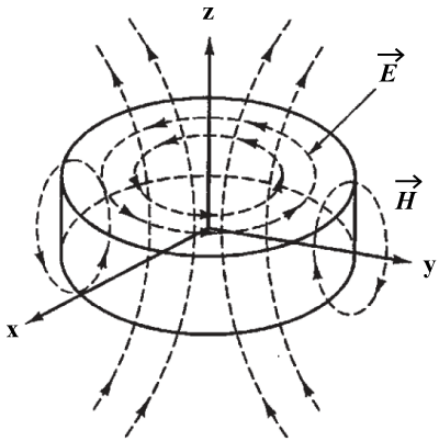

Figure 2.4: Field distribution in $TE_{01\delta}$ mode

The most common mode in a dielectric resonator is $TE_{01\delta}$ mode, in cylindrical resonator, or $TE_{11\delta}$ mode, in rectangular resonator. The $TE_{01\delta}$ mode is classified as the fundamental mode due to the fact that for certain diameter/length ratios

it has the lowest resonant frequency [28]. Field distribution for $TE_{01\delta}$ mode is illustrated in Fig.2.4 [20].

2.3.3 Quality Factor

The quality factor, commonly expressed as the Q factor, defines a relation between the resonant circuit's capacity for electromagnetic storage with its energy dissipation through heat. Resonator bandwidth is inversely proportional to Q factor. Thus, high Q factor resonators have narrow bandwidths, as for all microwave resonators [29, 11].

Q factor is defined by

$$Q = 2\pi * \frac{maximum\,energy\,storage\,during\,a\,cycle}{average\,energy\,dissipated\,per\,cycle}$$

$$Q = \frac{2\pi * W_0}{PT} = \frac{\omega * W_0}{P}$$

where W_0 is stored energy, P is dissipated power, ω_0 is resonant radian frequency and T is period, equal to $\frac{2\pi}{\omega_0}$.

The following numerical example illustrates the high energy confinement ratio of the dielectric resonator: In $TE_{01\delta}$ mode, when the relative dielectric constant is around 40, more than 95% of the electric energy and over 60% of magnetic energy is conserved within the resonator [29].

The name quality factor used by the manufacturers of dielectric ceramics, often does not correspond to the classical Q factor notion described above, therefore it should be distinguished [31]. It is also common to describe the dielectric materials by their $Q * f$ products, from which the user can deduce the approximate Q-factor at the intended frequency of operation.

The branded quality factor typically is the reciprocal of the dielectric loss tangent, $\tan\delta$. The dielectric loss tangent of a material quantitatively denotes the dissipation of the energy due to physical processes like electrical conduction,

dielectric resonance, dielectric relaxation and loss originating from nonlinear processes [31].

The sum of the intrinsic and extrinsic losses gives the total dielectric loss. Crystal structure dependent losses in the perfect crystals, which could be described by the interaction of the phonon system with the electric field, constitute the intrinsic type of losses. These are also dependent on the frequency and the temperature [31].

The loss of an ideally pure and defect-free material gives the lower limit of losses and is characterized by the intrinsic losses. Imperfections within the crystal lattice however, contribute extrinsic type of losses. Impurities, structural defects, porosity, micro-cracks, dislocation, vacancies and dopant atoms cause these extrinsic losses and theoretically be eliminated or minimized by material processing [31].

Type of defect affects the frequency and temperature dependence of the loss it causes. Similar variation of dependence is also reported to be observed for crystals with varying symmetry groups. The effects of material properties over electrical performance are briefly discussed in this chapter [31].

There are four types of losses that can be observed in a microwave resonator: Dielectric, Conduction, Radiation, and External.

The quality factors for dielectric, conduction and radiation types of losses are respectively given by [31]

$$Q_d = 2\pi \frac{W_{1]}}{P_d T} = \frac{\omega_0 W_1}{P_d}$$

$$Q_c = \frac{\omega_0 W_1}{P_c}$$

$$Q_r = \frac{\omega_0 W_1}{P_r}$$

where W_1 is the total stored electric energy in the resonator, ω_0 is the angular resonant frequency, P_d, P_c, $and\, P_r$ represent the dielectric, conductor and radiation power dissipated respectively and

$$T = \frac{2\pi}{\omega 0}$$

Dielectric loss could also be expressed in terms of the loss tangent. The loss tangent for a dielectric material is defined as

$$\tan\delta = \frac{\sigma}{\omega\epsilon_0\epsilon_r}$$

where $\epsilon_0\epsilon_r$ is the dielectric constant of the material and σ is conductivity of the medium.

Dielectric quality factor is

$$Q_d = \frac{\omega_0 W}{P_d} = \frac{\omega_0\epsilon\int|E^2|dV}{\sigma\int|E^2|dV} = \frac{\omega 0\epsilon}{\sigma} = \frac{1}{\tan\delta}$$

Conductor quality factor is

$$Q_c = \frac{\omega_0 W}{P_c}$$

where W is the maximum stored energy and P_c is the conductor power loss.

Radiation quality factor is

$$Q_r = \frac{\omega_0 W}{P_r}$$

where P_r is the radiated power.

Combination of these given Q factors give a quality factor that represents the total quality factor of the resonator with regard to internal losses [31, 29]. This

combination is denoted as *Unloaded Q factor* and is usually represented with Q_0 or Q_u,

$$\frac{1}{Q_0} = \frac{1}{Q_c} + \frac{1}{Q_d} + \frac{1}{Q_r}$$

where $\frac{1}{Q_d}$ is dielectric loss, $\frac{1}{Q_c}$ conductivity loss due to shielding plates and $\frac{1}{Q_r}$ is the radiation loss.

In order to limit the effects of the energy that is not conserved within the resonator, a metal shield that is usually aluminum is used to enclose the dielectric resonator. Thus the radiation loss is prevented. Therefore if the cavity is enclosed, radiation loss term could be neglected [31, 29].

Design of the shielded cavity not only affects the overall loss of the system and hence the quality factor; but also has impacts on resonance characteristics, like insertion loss, spectral purity, temperature stability and spurious mode rejection [31].

The resonant frequency rises if the metal walls are put closer to the dielectric. According to cavity perturbation theory, inward movement of a metal wall of a resonant cavity causes a decrease in the resonant frequency if the stored energy of the displaced field is predominantly electric. If the stored energy close to the metal wall is mostly magnetic, an increase occurs in the resonant frequency, however. TE_{01} mode is the latter case [29]. This phenomenon is also exploited for the mechanical tuning of the resonator's resonance frequency. Tuning characteristics are explained in the following sections.

From the end user point of view, unloaded Q factor is a sufficient figure of merit for design and it is used primarily as the basis for the design of coupling schemes.

If the application requires further analysis on the origin of internal losses, conductor losses could be accounted for by using following relation [31].

A geometric factor G is introduced as

$$G = \omega \frac{\int\int\int \mu_0 |H|^2 dv}{\int\int |H_t|^2 dS}$$

where μ_0 is the permeability of the resonator. The conductor quality factor is then related by

$$\frac{1}{Q_c} = \frac{R_s}{G}$$

where Rs is the surface resistance of the metallic cavity structure enclosing the DR.

Losses of external type are due to coupling. Coupling is established by bringing a conductor close to the resonator in order to introduce an electromagnetic field in the resonator; while the conductor may vary as loop, microstrip or stripline, depending on the preferred method.

External Q factor, Q_e, represents the losses due to the load circuit that uses the resonator via coupling. The *loaded Q factor* term is used to denote the overall Q factor and it includes both internal and external losses [31, 29].

$$\frac{1}{Q_L} = \frac{1}{Q_0} + \frac{1}{Q_e}$$

It is easily seen that the lowest loss value dominates the overall loss.

Studies suggest that excitation of Whispering Gallery modes (WGMs) reduces the radiation and conductor losses to negligible levels at microwave frequencies since the entire fields are confined within the resonator; thus minimizes the internal losses and maximizes the unloaded Q factor [31].

Propagation constant along the z axis is very small in WGMs; hence the spurious modes are suppressed with high performance, because they leak out axially. Classification of WGM DRs is done with regard to the transverse fields. In $WGE_{n,m,l}$ DRs, electric field is essentially transverse, while in $WGH_{n,m,l}$ DRs it is

axial. n, m, and 1 denote the azimuthal, radial, and axial variations, respectively [31].

The number of modes in a bandwidth increases with the diameter of the resonator. Therefore the frequency interval between two successive modes is large if the diameter is small.

Methods of excitation of WGMs differ depending on the desired application frequency band. Electric or magnetic dipoles can be used in the low frequency range. In higher frequencies, either dielectric image waveguides or microstrip transmission lines are used. The former excites stationary modes, while the latter are able to excite traveling WGMs [31].

As described previously, physical implementation concerns arise as the frequency gets higher and dimensions of the resonator gets smaller. In WGM method the dimensions are not linearly dependent on frequency and corresponding dimensions are much larger for the same resonant frequency than that of TE_{01} mode, so this higher level of integration also makes it attractive in high frequency applications [31, 28].

2.3.4 Frequency and Phase Response of the Dielectric Resonator

The following analysis of the transfer function is summarized from [29, 2].

Differential equation that describes the resonator circuit's behavior could be obtained by the manipulation of Maxwell equations:

$$f(t) = \frac{d^2v}{dt} + 2\sigma\frac{dv}{dt} + \omega_0^2$$

If a $\sigma \neq 0$ value exists, then the resonator has losses. Transfer function of the given system is:

$$T(s) = \frac{1}{s^2 + 2\sigma s + \omega_0^2}$$

$$T(s) = \frac{j}{2\omega_L}\left(\frac{1}{s + \sigma + j\omega_L} - \frac{1}{s + \sigma - j\omega_L}\right)$$

where ω_L denotes the loaded natural frequency and equals to:

$$\omega_L = \sqrt{\omega_0^2 - \sigma^2}$$

Implication of this equation is that the presence of loss changes the resonant frequency, which is called frequency pulling due to loss.

The natural response of the differential equation is

$$v(t) = V \exp(-\sigma t) \sin(\omega_L t)$$

The average power P in the system is

$$P = -\frac{dW}{dt} = 2\sigma W$$

Q is then

$$Q = \frac{\omega_0}{2\sigma}$$

Inserting this equation into ω_L expression gives

$$\omega_L = \omega_0 \sqrt{1 - \frac{1}{4Q^2}}$$

Differential equation can also be rewritten as

$$f(t) = \frac{d^2v}{dt^2} + \frac{\omega_0}{Q}\frac{dv}{dt} + \omega_0^2 v$$

For an ideal resonator, i.e., Q approaches to infinity, term with the first derivative becomes zero. Q is finite in practice though, so the first derivative is kept.

Transfer function $T(s = j\omega)$ becomes

$$T(\omega) = \frac{1}{\omega_0^2 - \omega^2 + \frac{j\omega\omega_0}{Q_0}}$$

$$= \frac{1}{j\frac{\omega\omega_0}{Q}\left[1 + jQ\left(\frac{\omega}{\omega_0} - \frac{\omega_0}{\omega}\right)\right]}$$

Term with ω dependence is

$$\frac{\omega}{\omega_0} - \frac{\omega_0}{\omega} = \left(\frac{\omega - \omega_0}{\omega_0}\right)\left(\frac{\omega_0}{\omega} + 1\right)$$

Since high Q factor means narrow bandwidth, ω is very close to ω_0, therefore the second term on the right hand side of the equation approximates to 2. Then,

$$\frac{\omega}{\omega_0} - \frac{\omega_0}{\omega} \approx 2\left(\frac{\omega - \omega_0}{\omega_0}\right) = 2\delta$$

where δ denotes the frequency tuning parameter. Transfer function under this approximation is then

$$T(\omega) = \frac{-j\frac{Q}{\omega\omega_0}}{1 + j2Q\delta}$$

magnitude of $T(\omega)$ is a bell-shaped curve, which is heavily dependent on Q.

The half power bandwidth B is defined as the frequency span $\Delta\omega$, of which upper and lower frequency bounds satisfy the following equation

$$|T(\omega)| = \frac{1}{\sqrt{2}}|T(\omega|)$$

Inserting the approximated transfer function expression,

$$\frac{\frac{Q}{\omega\omega_0}}{\sqrt{1+4Q^2\delta^2}} = \frac{1}{\sqrt{2}}\frac{Q}{\omega_0'2}$$

when $4Q^2\delta^2 = 1$ the equation holds. Therefore,

$$\delta = \pm\frac{1}{2Q}$$

$$\frac{\omega_i - \omega_0}{\omega_0} = \pm\frac{1}{2Q},\ i = 1, 2$$

$$B = \Delta\omega = |\omega_1 - \omega_2| \approx \frac{\omega_0}{Q} = 2\delta$$

In other words, the loaded resonant frequency and bandwidth that is approximated under high Q assumption can be inferred from the Q factor:

$$Q = \frac{\omega_0}{\Delta\omega} = \frac{f_0}{\Delta f}$$

Chapter 3

Design Method

3.1 Previous Work

3.1.1 1/f Noise Reduction

Since the flicker noise, or 1/f noise is the phase noise performance bottleneck in most cases, techniques aiming to reduce it have been studied extensively. Methods developed to enhance the flicker noise performance mainly fall into two categories: Circuit configurations that externally modify the flicker noise behavior and alterations of the internal device structure that intend to suppress the effects of the physical phenomena causing the flicker noise.

3.1.1.1 Device Level Methods

Introducing fluorine in order to reduce the flicker noise is a common device-level method. It's been found that through the doping of fluorine, improvements can be made in hot carriers, interfacial and breakdown characteristics. Evident contributions of this manipulation can also be maximized through setting the optimum dose, doping locations and other process flow parameters [32].

There also exist methods that exploit the customary design process of MMICs, such as setting the impedance presented to the source to rise at low frequencies. Obviously a similar approach is much more difficult to implement with discrete amplifiers due to the necessity of very low parasitic [13].

Increasing the physical size of the amplifier's active region also is an alternative, since the flicker noise is inversely proportional to it [2].

A statistical model for small MOSFETs, which defines the area dependence of flicker noise mean and variation, is proposed in [9]. In this work, it's also been observed that flicker noise variability shows a log normal distribution.

3.1.1.2 Circuit Level Methods

Bipolar amplifiers that operate at lower frequencies like HF - VHF band have a better 1/f phase noise performance than that of microwave amplifiers. A delicate circuit configuration called transposed gain amplifier makes use of this potential by transposing the low frequency gain up to microwave frequencies through down-conversion, amplification and up-conversion operations. Introduction of a delay line between the two mixers could also be used to make the resulting phase noise performance independent from the local oscillator's spectral purity [2, 23, 13].

Feed-forward amplifiers also suppress the flicker noise. Signal is coupled onto two paths with a certain coupling ratio, one of them is fed to the amplifier, and the other is delayed by using a delay line in this configuration. When utilizing a feed-forward amplifier as the active device part of an oscillator, it should be noted that the gain control, which is necessary to sustain the oscillation amplitude at a certain level, should not be the duty of the feed-forward amplifier. Because the lower flicker noise advantage would be lost or insignificant, if the feed-forward amplifier is operated in saturation for gain limiting purposes. A separate amplitude limiter with plausible 1/f noise should be used to saturate the gain. A Schottky-diode limiter could be a good candidate because of its lower 1/f noise than that of microwave amplifiers [2, 23]. Phase noise suppression achieved using this configuration can be as large as 20 dB, at the cost of increased circuit

complexity [13].

A noise correction control loop could be utilized by measuring the instantaneous phase fluctuation with a phase detector and using this information as the error signal. The residual phase noise is mostly due to the phase detector in such a configuration, which is also known as feedback degeneration amplifier. The main idea behind this approach is to get a lower 1/f noise through the use of a double-balanced mixer as the phase detector, thus eliminating the amplifier's relatively higher phase noise, in a similar manner with transposed gain amplifier configuration. Utilizing a bridge phase detector instead of the double-balanced mixer is also possible. It has a low 1/f noise that is limited by the variable attenuator and variable phase shifter balancing the bridge [2].

An amplifier structure that consists of an m-way power divider, m parallel amplifiers and an m-way power combiner is called a parallel amplifier. A merit of this configuration is enabling of the power extension of a given technology, considering the fact that each branch contributes 1/m of the output power, upper limit for power output is multiplied by m, ignoring the dissipative losses at the divider. Combining m independent noises, along with the dissipative losses at the divider, results in a higher white noise at the output in comparison with that of a branch yet. However, considering the flicker noise, due to input power division, a noise reduction is realized [2].

Incorporation of techniques like frequency locked loop, phase locked loop etc. has enabled the design of ultra low noise oscillators with phase noise performances approaching thermal noise limits. SSB phase noise of such a sapphire dielectric resonator oscillator operating at 9 GHz frequency is the lowest yet reported, which is -157 dBc/Hz at 1 kHz offset from the carrier [33].

A simple low-pass filter with DC blocking is added between output and input of the circuit in [34]. An improvement of 9 dB at 1 MHz offset frequency is reported for a VCO at 1.57 GHz. Measured results show that the improvement is residual, i.e. the phase noise is better at all offset frequencies observed. Moreover, as the offset frequency increases, the amount of improvement increases.

Implementing low frequency feedback in amplifiers for the purpose of suppressing both intermodulation products and phase noise is proposed in [35]. Although the work is focused on amplifiers, results indicate low frequency noise suppression and hence improved phase noise performance.

Some studies focused on accurate noise modeling of the FET devices. A simple model in which gate voltage noise generator is in series with a noiseless device is proposed in [36]. Reducing the sensitivity of gate-to-source voltage, which is reported as the primary responsible element for the upconversion of low frequency noise is another modeling approach [27].

3.2 Design Phases

In this section, design steps of a low phase noise DRO is described.

Upon selection of a proper device, circuit configurations are studied and the most suitable configuration is determined. Then, the bias networks are EM simulated for maximizing the post-production accuracy of the design.

Phase noise of the circuit is then minimized by isolating the amplitude and phase fluctuations, as predicted by Kurokawa model. Optimum resonator coupling described by Everard model is added to this approach. An insightful and responsive simulation setup that combines both aspects is proposed and explained.

After the RF/EM design of the oscillator is completed, low frequency feedback networks are introduced for suppression of flicker noise and results are presented in the next chapter.

3.2.1 Device Selection

Silicon bipolar transistors are known to have the lowest $1/f$ noise performance.

GaN HEMTs have high flicker noise corner and poor low frequency noise

behavior, therefore GaN oscillators are outperformed by Si and GaAs oscillators, in terms of phase noise [37].

It is advised to use devices with low f_T, which is around two times of the operating frequency [12, 26]. Although there is no reasoning behind this reported experimental advice, it is consistent with the claim that the lowest 1/f noise is possible when the usability of the device has an upper limit that is no more than an octave above the frequency of oscillation. The transistor's S_{21} parameters should be smaller than unity at this upper frequency [14].

ATF-36077 pHEMT device from Avago Technologies and CF004-01 GaAs MESFET device from Mimix Broadband are used. Both devices have nonlinear models in the Agilent ADS library. Availability and product support should be of concern in designing for practical applications, ATF-36077 has been discontinued during the thesis work, as an example.

3.2.2 Bias Point and Bias Networks

Biasing the active device using transmission line networks gives significantly better phase noise performance than using lumped-elements [38].

DC block at the output node was initially implemented by a microstrip coupled-line structure. However as the substrate thickness decreases it becomes much difficult to satisfy both frequency response and manufacturing requirements, i.e. bandwidth is narrow and high impedance lines and proximity between coupling arms become too thin. As the features get smaller, the design becomes more prone to errors originating from manufacturing tolerances.

In some designs, insertion loss of the coupled-line DC block severely affected the close-loop gain, even though it was kept smaller than 1 dB. Therefore it is decided that the degradation on DC and low frequency performance of the circuit would be insignificant compared to that of operating frequency band response.

The operating point of the device is also effective on the phase noise performance. From the noise process view; it is claimed that since the noise is a fixed level, phase noise decreases with increasing power level [39, 15].

However as the current increases, upconversion of low frequency noise increases as well as the output power, due to increased nonlinearity. So it's not clear whether the phase noise increases with device current [11, 14, 12]. Therefore it might be a viable solution to keep the bias voltage higher (drain to source/drain to gate/source to gate, depending on configuration) while limiting the current not to exceed typical operation values too much.

It is obvious that stability of the device should be main parameter when selecting the operating point. Although configuration and feedback structures affect significantly, bias points that make a device unstable are usually a small subset of all possible bias points. Considering this device dependency, it can be concluded that the bias point for each design should be carefully selected with trial and error.

Device performances are compared with respect to bias points, however the observation of bias dependence is not main concern.

3.2.3 Circuit Configuration

The effects of choosing the common base/common gate, common drain/common collector, or common source/common emitter circuit configurations on phase noise performance are not widely studied in literature. Investigated devices mostly operate in common source or common base configuration.

In common source configuration, feedback capacitance from input to output is equal to gate-to-drain capacitance, which is relatively small compared to other capacitance values in the FET device. In common gate configuration, input impedance is equal to $1/g_m$ and unlike common source, it is not nearly pure capacitive. Matching input both to 50 ohms and to the optimum noise source impedance is possible. Consequently in amplifier applications, it is easier to

obtain a wider band, noise values in which are closer to F_{min} in this configuration [40, 12, 41].

Feedback capacitance of common drain configuration, which is also known as source-follower, is modified by gate-to-source capacitance. Input impedance is quite high and output impedance is low [12].

Due to their smaller internal feedback capacitance, common emitter and common source configurations are known to be inherently more stable than common gate/common base and the common drain/common collector configurations, while common gate and common base are known to have broader band. A feedback inductance added to the gate or base usually creates a reflection coefficient that is larger than unity, in relatively wider frequency band, making the device unstable [38].

Common-drain and common collector structures are well suited for negative-resistance oscillators, and common gate and common base are well suited for negative-conductance oscillators [12].

Gate-to-source capacitance is responsible for the up-conversion of the low frequency noise, while the nonlinear drain-to-source conductance has much less effect. Amplitude noise is primarily determined by the nonlinear transconductance [24].

Dependency of the frequency to gate-to-source voltage amplitude is modeled and reduced in [27].

Oscillators are built by implementing all three topologies. Power output, harmonics and phase noise performances are reported and compared.

3.2.4 Stability Analysis

ATF-36077 device is biased in common gate configuration with an external feedback element in gate port. Bias point is chosen as $V_{DS} = 2.5\,V$, $I_{DS} = 10\,mA$.

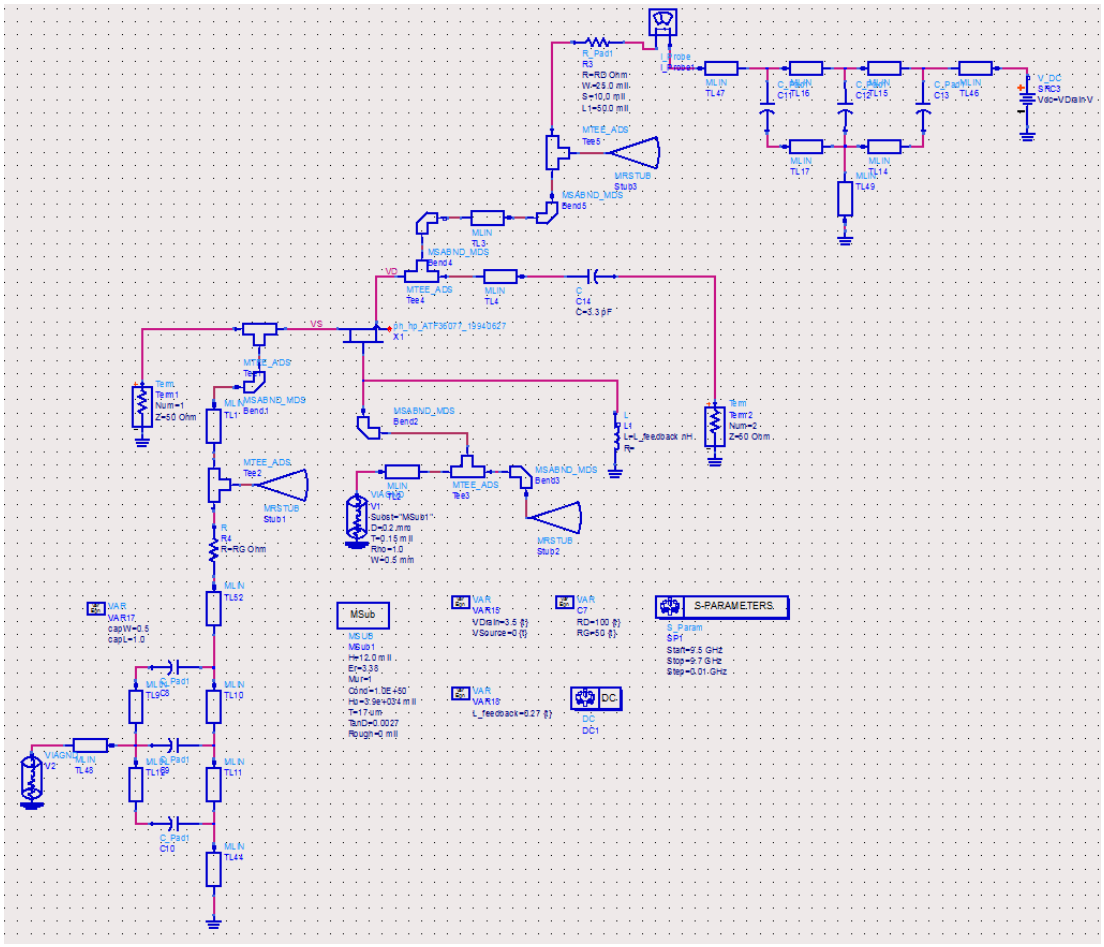

Figure 3.1: Device with feedback stub

Two identical circuits are built. The first one, shown in Fig.3.1, has a lumped inductor as feedback element. Second circuit, which is not shown in the figure, has an open stub. Inductance value of the lumped inductor is used for tuning the first circuit's stability. Width and the length values of the open stub are set accordingly, to mimic the behavior of the lumped inductor.

DC operation point and four port s-parameters are given in Fig.3.2. It is seen that DC bias point is approximately obtained. Stability factor μ is measured as -0.958.

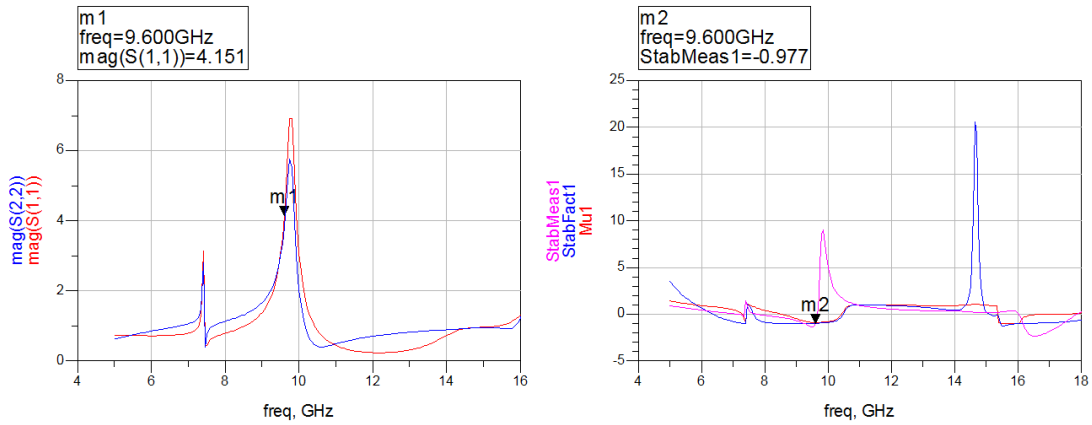

Figure 3.2: Stability analysis of the device with feedback

3.2.5 Electromagnetic Simulations and EM/Circuit Co-Simulations

It is well known that, EM simulation results of printed microstrip structures could deviate from that of RF simulation results. Depending on the application, it could be imperative to run EM simulations on initial bias networks, and to update and verify the circuit accordingly prior to design input and output matching networks.

Magnitude of the deviations between RF and EM simulations is observed to reach up to the order of hundreds of MHz. Inconsistencies are mostly observed in the simulation results of radial stubs that are used to provide RF chokes in bias networks. Fringing field effects that are approximated in RF simulator are ascribed for these.

Once the circuit's configuration, operation point, and feedback structure that makes the circuit optimally unstable -if necessary- are decided, the bias and feedback networks should be characterized by EM simulations.

Even slight frequency, phase, or magnitude shifts in the behavior of these networks, could make the stability of the device , hence the RF performance could be significantly affected.

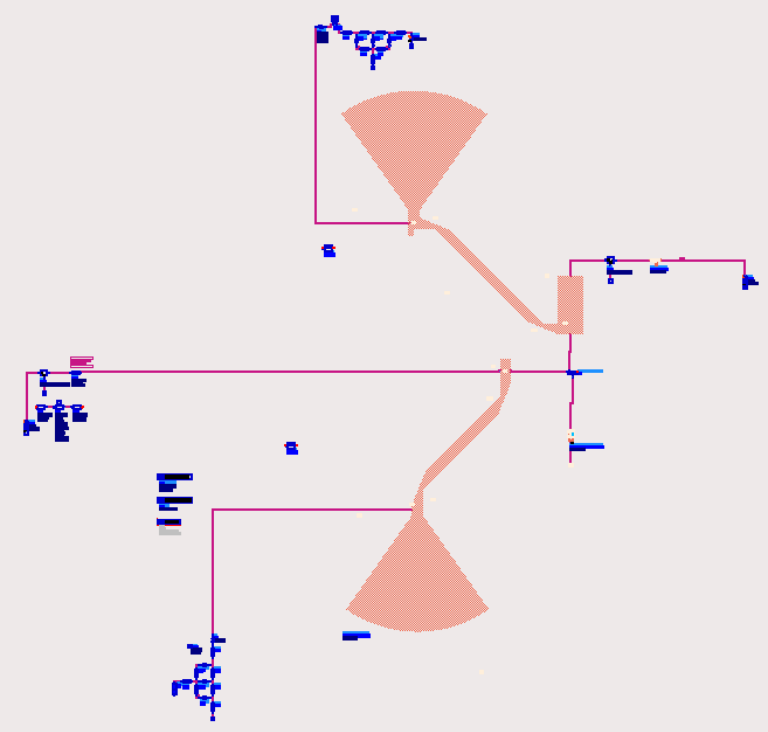

Figure 3.3: A design example that uses EM component

3.2.6 Resonator Simulation

Coupling of a dielectric resonator to microstrip or loop structures in a cavity is a three-dimensional electromagnetic problem. Contrary to AWR Microwave Office tool, Agilent ADS has no integrated 3D EM simulator engine. User should either measure the frequency response of the resonator, or model the desired resonator structure in a 3D EM simulator software and import the resulting s-parameters, or rely on the simple ADS model that is available in the standard library.

In ADS, microstrip coupled dielectric resonator element is modeled as a parallel RLC network, as described in [29].

Inherent weakness of this modeling approach is that the required distance between the resonator and the microstrip, one of the most important physical design parameters is unavailable at the design time. However, designing the circuit based on this empirical "coupling coefficient" parameter has its advantages too. It is possible to design the rest of the oscillator for the optimum value of the

coupling coefficient, without worrying about the phase noise degradation due to suboptimal resonator coupling, which could be quite significant.

It should be noted that if the resonator is to be coupled to two parallel microstrips, ADS dielectric resonator model is not valid. In this case the alternative to 3D EM simulation and physical measurement is using two transformers parallel to simple parallel RLC model of the resonator, through which the resonator couples to microstrips [20]. Turn ratios of the transformers define the coupling coefficient values of the resonator to the microstrips.

In this work the simple ADS model is used for two reasons: 1) To exploit the possibility of optimal design 2) To avoid complex and time consuming 3D EM simulations.

Considering the fact that the frequency response is a function of the resonator position, it is not viable to iterate spatially on the substrate through long EM simulations, which leads to a virtually infinite number of simulations. Instead, housing of the circuit is designed with two separate cavities which enable the resonator measurements at the integration time, to compensate the lack of a priori design information.

Loaded and unloaded Q factors of the resonator can be calculated using the magnitude of the transmission coefficient of the resonator [29].

A quantity name x is defined in the following way

$$x(dB) = 3 - 10log(1 + 10^{-0.1L0})$$

where x is added to minimum point of the insertion loss for the calculation of loaded Q, and is subtracted from the maximum, ideally zero, for the calculation o unloaded Q.

Dielectric resonator is simulated using the ADS model element, as explained previously. As transmission line is terminated with its characteristic impedance, length of it does not affect the coupling.

Substrate is chosen as Rogers RO4003C, with thickness of 12 mils. Resonant frequency dependence on substrate dielectric constant and thickness is significant, on the order of tens of MHz.

Resonator insertion loss is set to 6 dB by setting the coupling coefficient to 1 and x parameter defined above is obtained from the simulation results and given in Fig.3.4.

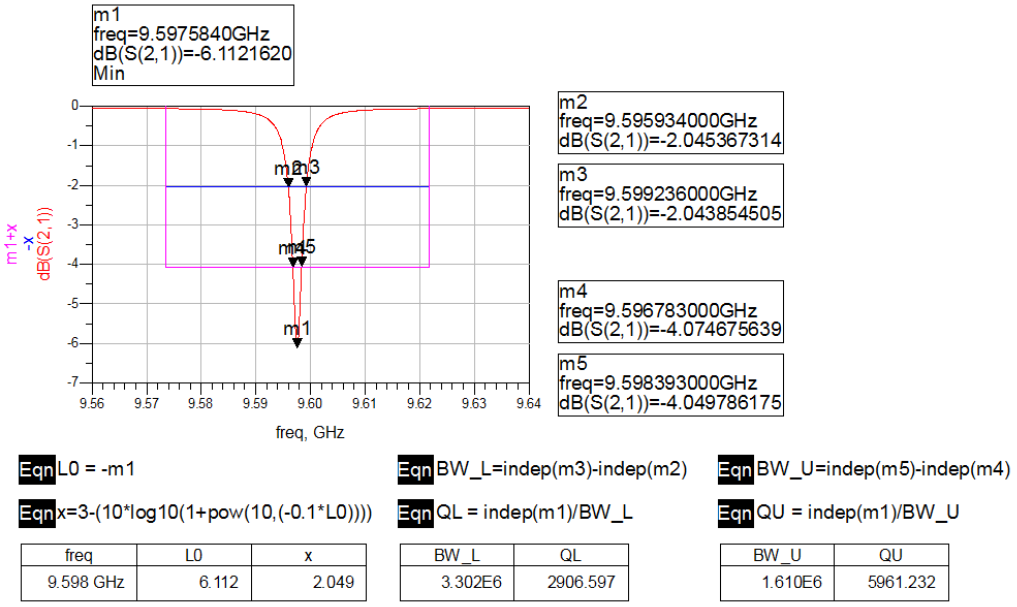

freq	L0	x
9.598 GHz	6.112	2.049

BW_L	QL
3.302E6	2906.597

BW_U	QU
1.610E6	5961.232

Figure 3.4: Simulation results of the dielectric resonator coupled to microstrip

Simulation results suggest an unloaded Q of 5961 and a loaded Q of 2906.

3.2.7 Output Matching

As explained previously, satisfying the oscillation conditions and phase noise characteristics depend on the input impedance of the active device, i.e. the impedance seen by the resonator. Therefore both the amount of the negative resistance seen in this port and its relation to the resonator's reflection coefficient are of utmost importance.

A simple formula for the design of output matching networks of oscillators is

to set the load resistance as one third of the negative resistance, and the load reactance equal to negative reactance. This basic procedure is based on small signal S-parameters analysis and hence does not account for the nonlinearity of the device [20].

Apart from the fact that it is not possible to calculate power output and harmonics levels beforehand using this method, it should be noted that the oscillation frequency usually deviates from its designated value due to the change in the negative reactance by signal level. It is safe to say that the possibility of the phase noise performance of the circuit to be suboptimal is quite high by using this technique [20]. Therefore such small signal approaches should only be utilized initially, if the design specifications require low phase noise.

In the resonator simulation subsection, it was shown that the frequency response of the resonator has an optimum for the best phase noise. Although being important, since the dielectric resonator is a passive device, its frequency response does not have much degree of freedom. Previously it was shown that for the best phase noise performance, reflection coefficients of resonator and the active device should be orthogonal to cancel fluctuations induced between phase and amplitude. In order to obtain such a relation, it is much useful to manipulate the active device input impedance rather than that of resonator, which is essentially a narrow band filter.

Output matching is thus the defining parameter for the oscillator. In the experiment, 50 Ohm termination at the output port of the device is removed and a large set of possible load impedances are swept via "Parameter Sweep" component, as shown in Fig.3.5.

Results show the input reflection coefficient values for each corresponding load impedance. There is not much information on the literature about the optimum negative resistance or conductance for the best phase noise. In [12], it is explained that higher negative resistance or conductance is used if fast starting and high output power are the design goals, whereas lower values result in better stability and noise performance. It is also advised to use a moderate negative resistance at the input port between -5 and -50 ohms, or between -0.2 and -0.02 mhos if

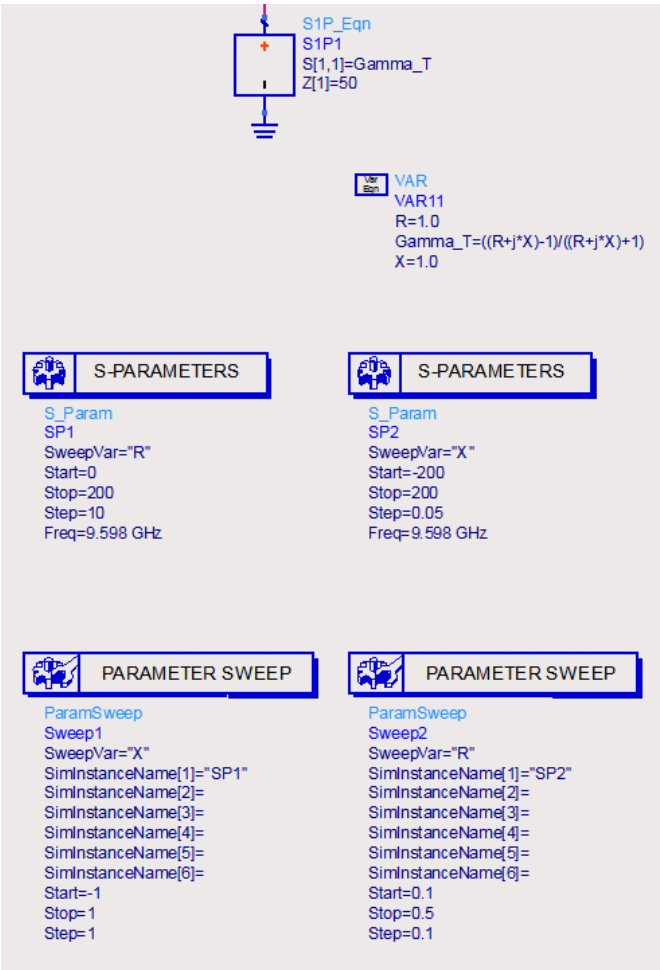

Figure 3.5: Output matching sweep simulation

negative conductance oscillator is being design. Negative resistance/conductance should be maximally flat with frequency and with little or no reactance. So a termination reflection coefficient is picked which provides sufficiently large input reflection coefficient and has low reactance.

Output is then matched from the selected impedance to 50 Ohm. Following the addition of the matching network, simulated input impedance and input reflection coefficient of the device is shown in Fig.3.6.

Negative impedance is $-21.256 + j5.185$, which has a real part adequate for the oscillation and small reactance.

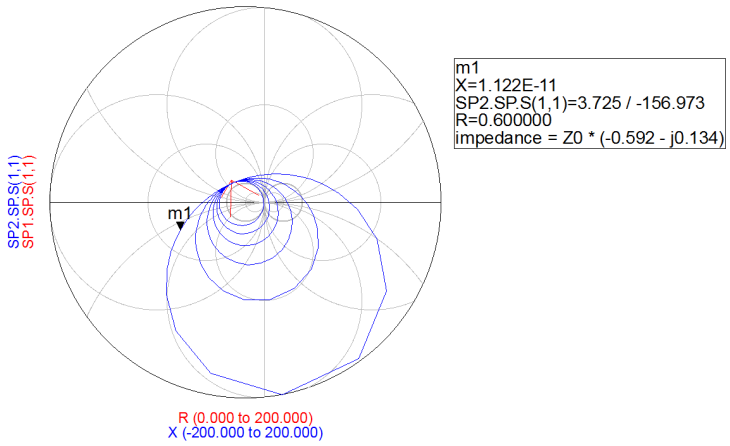

Figure 3.6: Corresponding input impedances loci for swept output impedances

It should be noted that this analysis is small signal and will be a basis for the following large signal analysis.

3.2.8 Large Signal Analysis and Optimization

Kurokawa oscillation condition describes an optimum for the phase noise as setting the large signal behavior of the device [25, 24].

Dielectric Resonator is modeled as parallel RLC tank circuit, therefore a DRO is a negative conductance oscillator. Optimization of the intersection of device and resonator trajectories at the operating point is reported to be one of the ultimate methods for obtaining low phase noise in [27], however the method was left out of the scope of their work.

It is reported that the RF voltage and power dependency of the input and output impedances are much less for FETs relative to the bipolar transistors. It is thus advisable for any oscillator design that uses a bipolar transistor as active device to create a test fixture and measure large signal S-parameters first [11].

The only tool for oscillator design in ADS is OscTest component. However this tool is quasi-linear, i.e. the simulation is small signal but all the active components are driven to their nonlinear bias conditions and then linearized [39].

Instead of inserting OscTest tool between the resonator port and transistor input port, resonator is simulated in small signal and active device is simulated in large signal. Then, the large signal behavior of the active device is plotted onto the resonator response and the circuit is tuned for optimum intersection, which is defined as perpendicular [25, 14, 24].

Both resonator and active device reflection coefficients could be set using this analysis method. Given simulation setup provides insight into the large signal behavior of the device, which is invisible to the user if OscTest or a similar tool is used.

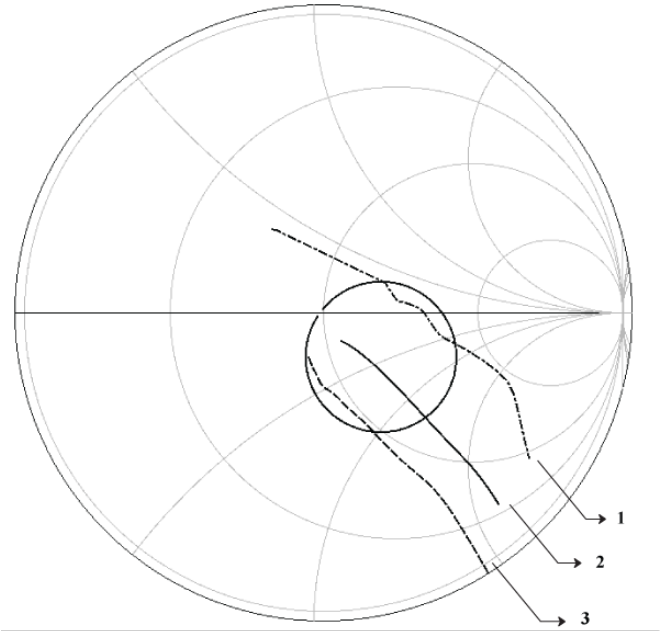

Figure 3.7: Tuning of transistor input reflection coefficient

A simple illustration of this tuning procedure is given in Fig.3.7. The circle represents the frequency response of the resonator. The lines intersecting the circle represent the inverted reflection coefficients of the transistors, seen from the port that is connected to the resonator. Each line corresponds to a circuit with different parameters and is denoted by a number.

2 has the optimal value, that is perpendicular to the circle. 3 is on a different bias point with all other parameters same, and 1 has a different output matching

network.

Note that however, the circle could be moved in clockwise or counter-clockwise direction for any given specific transistor reflection coefficient trajectory by simply adjusting the coupling microstrip's length. Individual best matches of the lines 1 and 3 are still suboptimal and for the sake of simplicity they are not shown here.

Nyquist test results of the same circuits obtained with OscTest port between 9 and 10 GHz are shown in Fig.3.8.

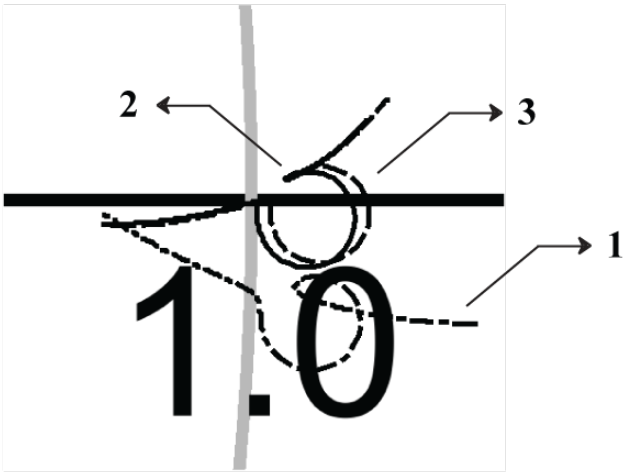

Figure 3.8: Nyquist test results of the same tuning

Recalling that the Nyquist oscillation criteria is to encircle $1 + j0$ point in clockwise direction and the oscillation frequency is the point at which the trajectory crosses the real axis; it is inferred that the circuit denoted by 1 is not going to oscillate in given frequency range. However this circuit oscillates as the other configurations, at 9.149 GHz frequency and with 9.1 dBm output power. Phase noise comparison of these three versions is given in Fig.3.9. Phase noise of the "optimal" version, denoted by 2, is better than others, around 10 dB.

As the example suggested, Nyquist test not only misleads about the circuit's oscillation, but also does not give any design feedback to the user. Two designs that exhibit 10 dB residual phase noise difference have almost the same Nyquist plots.

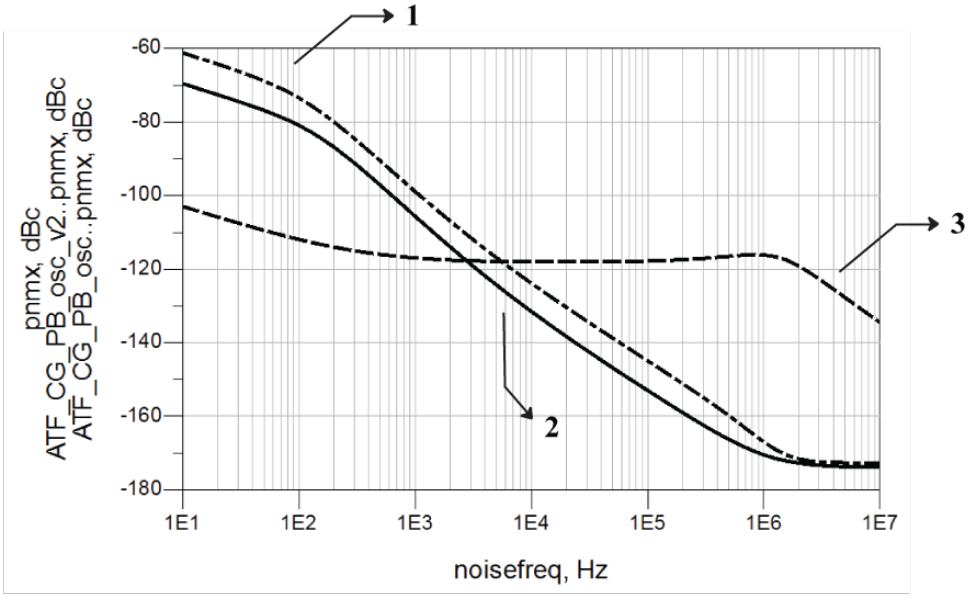

Figure 3.9: Phase noise comparison of circuits with varying input reflection coefficients

Chapter 4

Results

Dielectric Resonator Oscillator circuits with varying parameters are designed by following the methods described in previous chapter and are simulated with Harmonic Balance simulator in Agilent Advanced Design System software. Harmonic Balance simulation gives power output, harmonic levels and phase noise. In order to analyze the oscillator in time domain, transient simulations are also added.

Design parameters include devices, operating frequencies, configurations, and bias points. ATF-36077, a packaged pHEMT device and CF004-01, a chip GaAs MESFET are used as active devices. Both are biased at two operating points, hereafter they will be denoted as Low Noise Bias (LNB) and Power Bias (PB), respectively. Voltage and current values used for ATF-36077 are 1.5 V, 10 mA for LNB; and 2.5 V, 20 mA for PB. For CF004-01, values are 3V, 10 mA for LNB; and 6V, 25 mA for PB. Values are for output-to-grounded nodes and hence their names change depending on the configuration, e.g. they are named V_{DS} and I_{DS} in common-source configuration.

Two dielectric resonators are used with resonant frequencies around 9.15 GHz and 11.45 GHz.

Oscillators are designed with all three possible circuit configurations; common-source, common-gate, and common-drain. Naming convention that is adopted for

the distinction of oscillators is to use device-configuration-bias prefixes respectively, e.g. ATF_CS_LNB, or CF4_CG_PB.

4.1 Resonator Measurements

Although Agilent ADS accurately simulates the resonant frequency of a dielectric resonator without the need of 3D EM simulation, manufacturing tolerances could lead to frequency deviations. In critical applications tolerances could be kept tight; however the cost would be higher in parallel.

MDR-24 series dielectric resonator is used from MCV Technologies. The resonator is reported to have an unloaded Q factor greater than 16000 at 10 GHz, with dielectric constant between 24 ± 1. Frequency specification was conveyed to the manufacturer as 9.6 ± 0.5 GHz, for the sake of low cost.

The measurements of the resonator showed that the resonant frequency is around 9.15 GHz. Loaded and unloaded Q factor calculations described in [29] are also given in Fig.4.1.

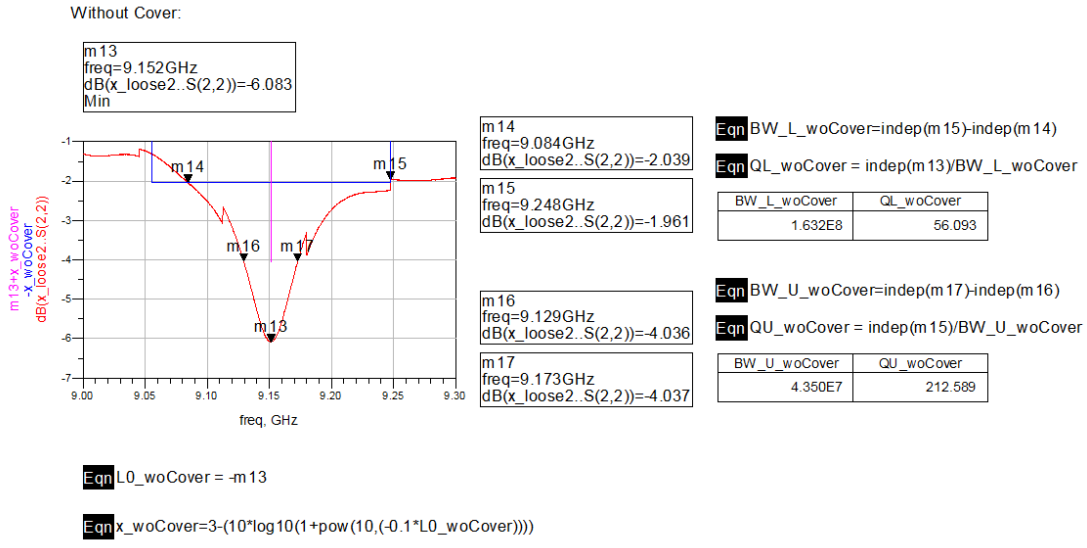

Figure 4.1: Measured resonator frequency response and quality factor calculations

In order to demonstrate the effect of shielding on quality factor and mechanical

tuning, a top cover plate is put on the test fixture with close proximity to the resonator. Measured response is given in Fig.4.2

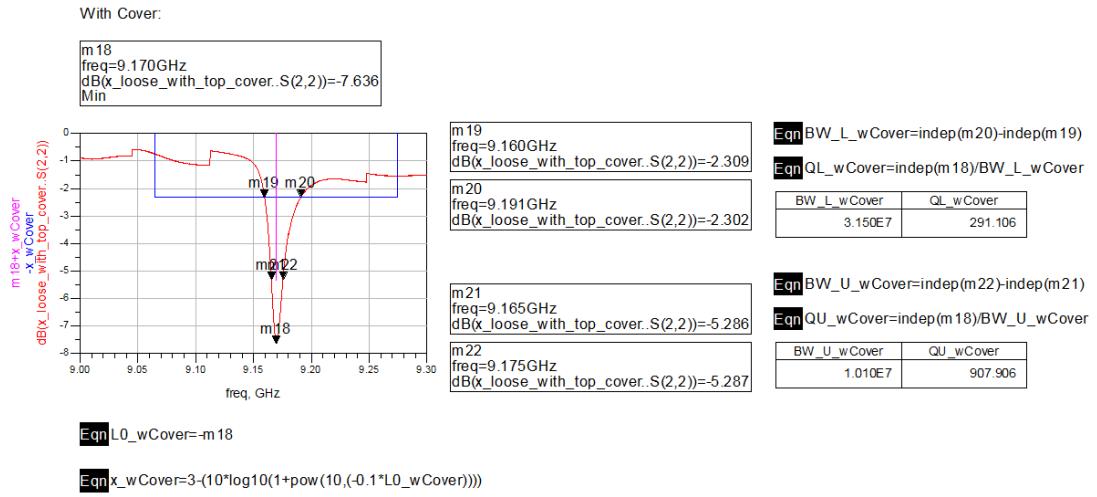

Figure 4.2: Measured resonator frequency response with top cover and quality factor calculations

It is seen that the frequency is slightly increased and the bandwidth is significantly narrowed, which means that the quality factor is increased. This increase is also quantitatively analyzed. Loaded Q factor is increased from 56 to 291.

Optimum resonator insertion loss for best phase noise is 6 dB, as reported in [23] and found in simulations. Therefore the resonator's proximity to the microstrip is set accordingly by simple trial and error method, in which the resonator's position is set in open cover fixture and the difference introduced by top cover plate is compensated thereafter.

Captured data was used to replace the ideal resonator element in previous designs. Since a frequency deviation is of concern, bias and RF feedback networks were revised accordingly. Large signal analysis was repeated with updated EM simulated components and output match network was redesigned.

Large signal input reflection coefficient of the revised circuit, measured data and the frequency response of an ideal resonator that is designed to imitate the actual resonator are shown in Fig.4.3.

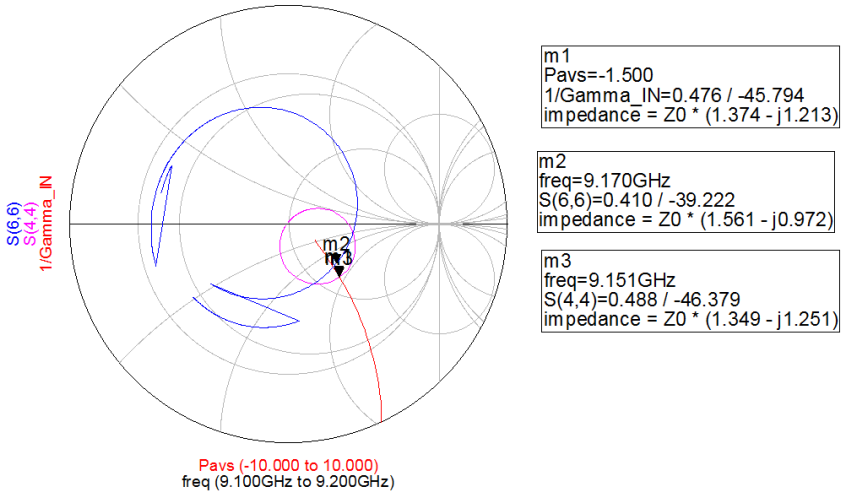

Figure 4.3: Large signal analysis of the device with measured resonator response

It is seen that the intersection is approximately set for optimum. Harmonic Balance simulation results show the oscillation at 9.162 GHz, with phase noise performance consistent with the oscillator designed by using ideal resonator model. Therefore the measurement results are used for further simulations described in this chapter.

4.2 Comparison of Devices, Circuit Configurations, and Bias

Simulation results of oscillators that are designed for operation at 9.15 GHz are summed in Table 4.1. f_{osc} and f_{tran} denote to the oscillation frequency (GHz), calculated by Harmonic Balance simulator and Transient simulator, respectively. H_1 is power output and H_2 is the level of second harmonic (both in dBm). The last four columns denote the phase noise levels at given frequency offsets (in dBc/Hz).

CF004-01 device did not oscillate in common drain configuration, while ATF-36077 oscillated. However, these common drain oscillators have poor phase

Table 4.1: Phase Noise Performance Comparisons

Osc	f_{osc}	f_{tran}	H_1	H_2	@100Hz	@1kHz	@10kHz	@100kHz
ATF_CD_LNB	9.150	9.228	-1.7	-14.5	-50.2	-61.0	-80.8	-100.8
ATF_CD_PB	9.150	9.207	5.208	-7.996	-40.4	-60.2	-80.2	-100.1
ATF_CS_LNB	9.151	9.313	1.7	-14.7	-74.8	-100	-126.5	-148.5
ATF_CS_PB	9.332	9.398	7.5	-26.2	-37.1	-54.1	-73.7	-93.74
ATF_CG_LNB	9.150	9.139	3.7	-20.8	-77.0	-100.5	-125.3	-146.2
ATF_CG_PB	9.150	9.140	10.0	-12.8	-80.9	-105.7	-131.5	-153.0
CF4_CD_LNB	-	-	-	-	-	-	-	-
CF4_CD_PB	-	-	-	-	-	-	-	-
CF4_CS_LNB	9.150	9.140	-3.7	-27.3	-86.7	-106.8	-126.8	-146.8
CF4_CS_PB	9.150	9.145	12.2	-21.6	-95.1	-114.0	-134.3	-154.2
CF4_CG_LNB	9.150	9.171	0.5	-21.9	-94.6	-111.3	-126.0	-145.9
CF4_CG_PB	9.151	9.142	3.0	-25.3	-96.5	-113.5	-127.2	-147

noise performance in both LNB and PB conditions. Relatively larger difference observed between the f_{osc} and f_{tran} frequencies could be an indicator of a frequency shift due to increased nonlinearity level. A similar effect is observed in ATF_CS_PB device. Oscillation frequency calculated by Harmonic Balance and Transient simulations are close, yet away from the resonance frequency. As in the case of CD oscillators, phase noise is quite high.

Common gate configuration shows good phase noise performance for both devices and for both bias points. Best phase noise performance away from the carrier is that of CF4_CS_PB, however the close-in noise performances of CG configurations are slightly better.

4.3 Effect of Resonator Coupling on Phase Noise

Everard's phase noise model defines an optimum for the ratio of the loaded Q to the unloaded Q [23]. Phase noise is lowest for the resonator insertion loss value of 6 dB. According to their observations, phase noise degrades for higher and lower insertion loss values, approximately linearly on a dB scale. At higher than 6 dB

insertion loss region, slope of the degradation is approximately 0.75, at lower than 6 dB insertion loss region the slope is approximately 4.

Resonator coupling simulation experiment results are consistent with findings of [23]. In Fig.4.4, phase noise performances of identical common-drain oscillator circuits with varying coupling coefficients are shown. Optimal value for insertion loss is found as 6 dB.

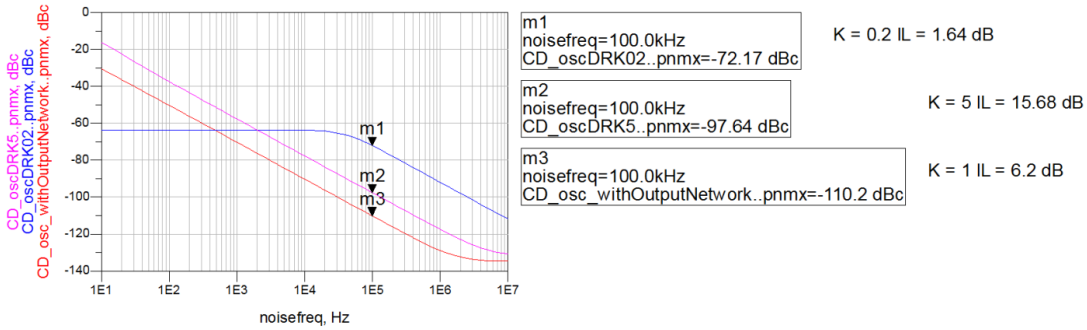

Figure 4.4: Simulated phase noise vs. resonator insertion loss

4.4 Large Signal Optimization

Simulation results clearly demonstrates the optimality of the phase noise performance depending on the coupling characteristics. Fig.4.5 shows the intersections of large signal input reflection coefficient trajectories and resonator response depending on the coupling line length. Corresponding phase noise results are listed in Table 4.2.

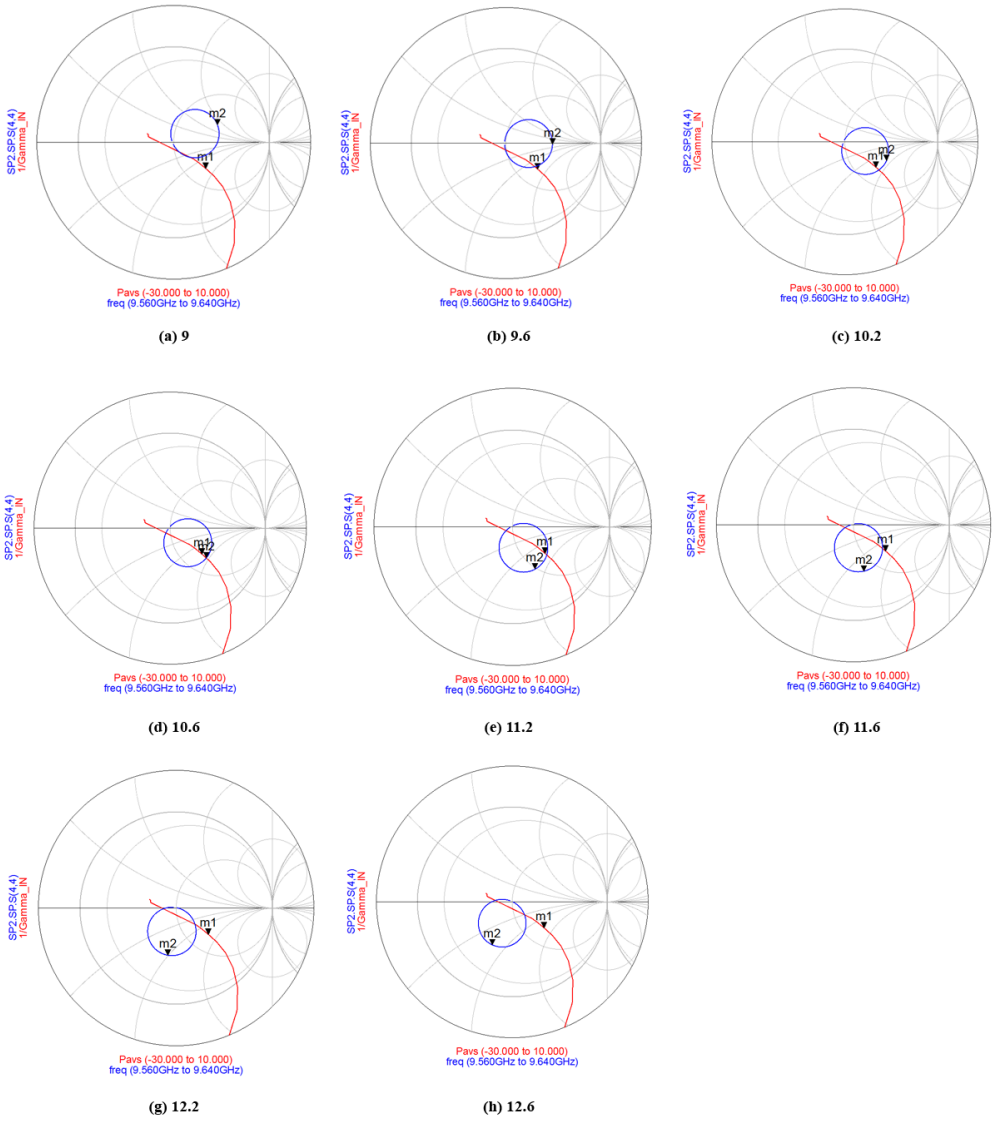

Figure 4.5: Varying coupling simulation results

Table 4.2: Phase Noise Degradation Depending on the Intersection Angles

Line Length in mm	PN @100 kHz (dBc/Hz)	PN Deviation(dB)
9	-127	-19
9.6	-140	-6
10.2	-145	-1
10.6	-146	0
11.2	-144	-2
11.6	-140	-6
12.2	-133	-13
12.6	-129	-18

This tuning process has two degrees of freedom, which are proximity of the resonator to the coupling microstrip and to the active device. Such a tuning procedure could be implemented when the oscillator is being built by experimentally changing the dielectric resonator's position. It should be noted however that, tuning of these two parameters do not necessarily result in optimum phase noise performance since the input reflection coefficient could not be measured or tuned in this approach. Results of suboptimal input reflection coefficient are illustrated in the previous chapter.

Large signal behavior of the transistor's input reflection coefficient is tuned by output matching network, RF feedback stubs if any, and bias point.

4.5 Low Frequency Feedback Techniques

4.5.1 Output-to-Input Low Frequency Feedback

Adding a Low Pass Filter (LPF) in the oscillation loop is reported to reduce the phase noise by suppressing the low frequency noise [24, 34].

Three identical oscillators with LPF networks inserted between Drain and Source terminals are simulated. Cut-off frequencies are varied as shown in Fig.4.6. Phase noise performances of these oscillators with feedback are significantly better than that of the one without feedback and are close to each other.

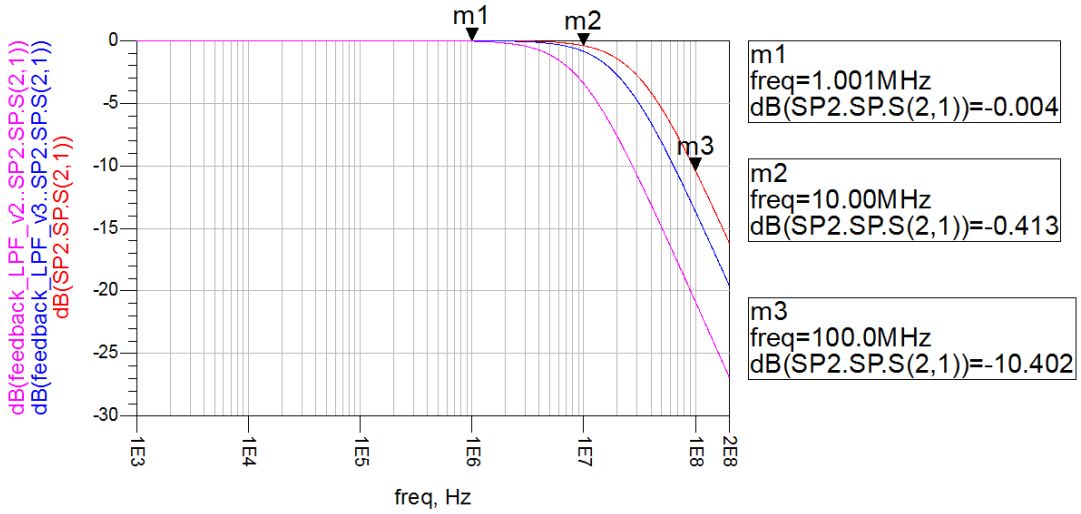

Figure 4.6: Comparison of the frequency responses of three alternative feedback filters

Simulated oscillators use FET and MESFET transistors. Since the flicker noise corner of this device family could be as high as a few MHz, cut-off frequency of LPF could be set intuitively around this level. However, simulations showed that the effective bandwidth of the low-pass feedback mechanism on the resulting phase noise spectrum is hard limited, i.e., it is useless to provide feedback for frequencies that are away from the carrier after a certain offset value. This is an expected result since the upconverted low frequency noise is effective at near-carrier frequencies, while the phase noise is dominated by the resonator's loaded quality factor at frequencies that are away from the carrier.

Harmonics are given in Fig.4.7.

Phase noise spectra are given in Fig.4.8

Feedback network significantly improved the near-carrier phase noise performance of the oscillator, with slight dependence of the cut-off frequency. Best phase noise performance is obtained when the filter with largest pass band is used. Improvement is around 6 dB at frequencies less then 100 Hz.

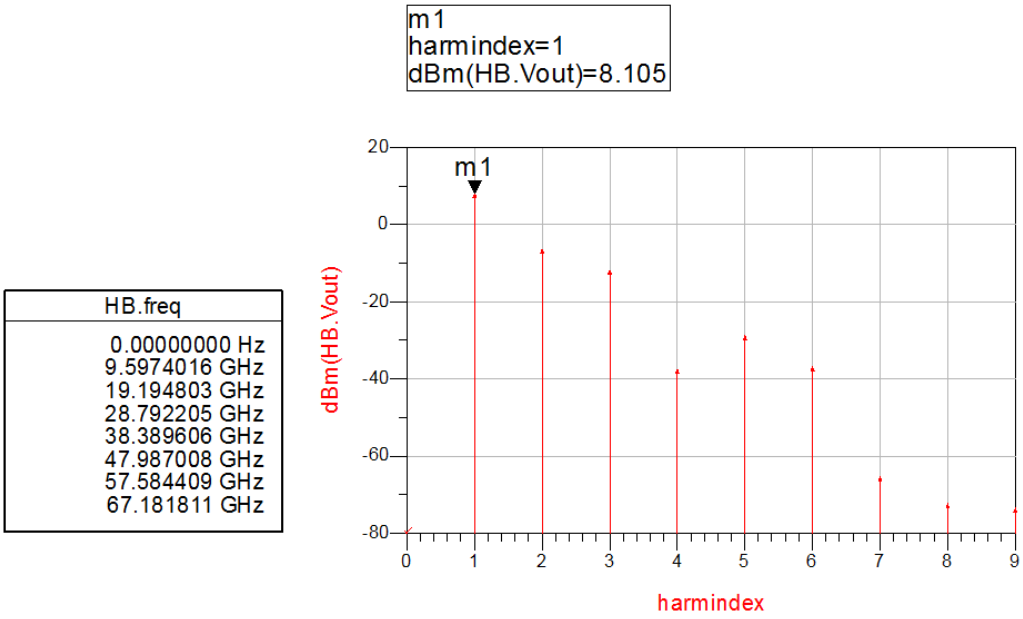

Figure 4.7: Harmonic Balance simulation results of the oscillator circuit with LPF feedback

Phase noise simulation tools in modern CAD tools are reported to give accurate and consistent results [39, 42]. In [42], difference between phase noise simulations and measurements are found to be insignificant at frequencies greater than 1 kHz offset.

Although introducing low pass feedback network to the oscillation loop is a known method, it could be argued that the accuracy of the simulation of near-carrier phase noise improvement would be limited; considering the fact that manufacturers usually don't provide flicker noise corner data and measuring flicker noise could be impractical because of the need for advanced instruments and complicated test fixture. However the results indicate that the improvement exceeds 40 dB at its most; is greater than 10 dB at 1 kHz offset, and gradually decays to 1 dB up to 10 kHz offset. So even if the improvement is erroneously calculated at lower offset frequencies due to simulator incapability, it is still significant in the 1-10 kHz bandwidth, in which the simulator is known to work accurately [42].

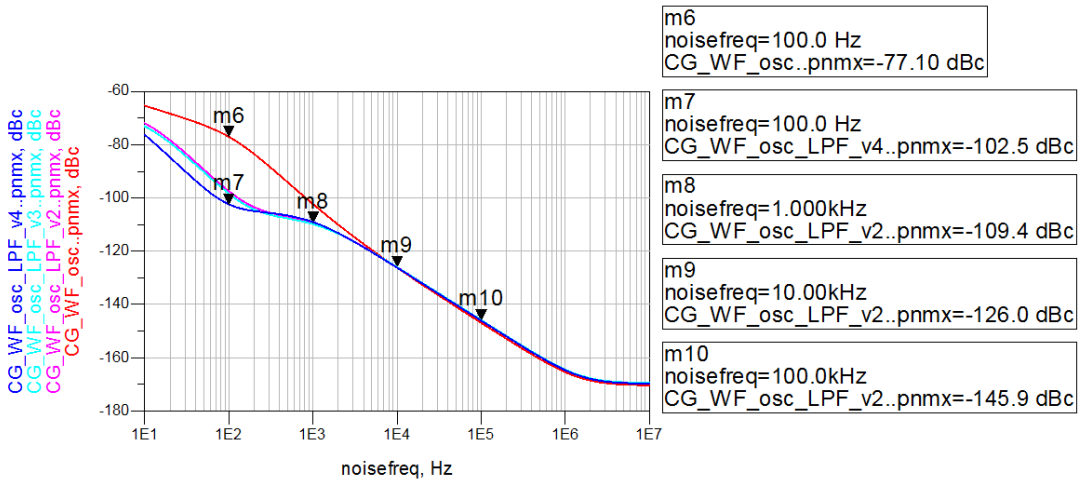

Figure 4.8: Phase noise comparison of the oscillators with and without feedback network

4.5.2 Complex Feedback Schemes

Low frequency feedback methods in the literature treat the transistor as a two-port device, and the feedback filter is inserted between output and input nodes. However, in a DRO circuit the flow of the low frequency band is not limited with output to input terminals' interconnection of the active device. The low frequency loops for a common-gate configuration are illustrated in Fig.4.9.

RFC blocks denote the RF chokes, which isolate the bias nodes from the operating frequency band. Loop 2 and 3 constitute the Loop 1, which is drain-to-source in common gate configuration. Assuming that the output is DC-blocked as shown in the Fig.4.9, there is one other contributing loop, which is shown as Loop 4.

Nonlinear behavior of the internal capacitances contribute to the upconversion of the low frequency noise[24, 27]. Hence individually filtering these capacitances by inserting filter network to loops 1,2, and 3 is investigated.

Since the best phase noise performance is obtained with common-gate oscillators in previous simulations, this configuration is picked for experimenting on the effectiveness of the low frequency feedback networks.

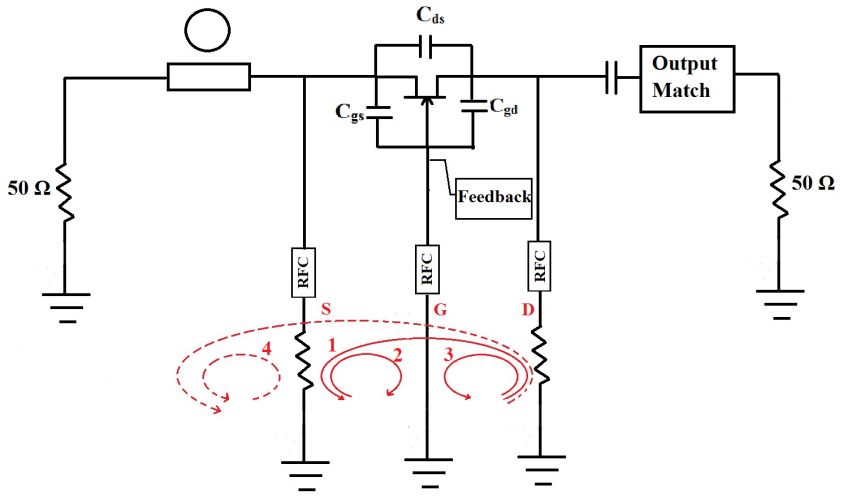

Figure 4.9: Low Frequency Loops in a Common-Gate DRO Circuit

Two types of filters are used. In order not to affect the bias point, both are designed with DC-blocking functionality. The former is a pure Low-Pass Filter shown in Fig.4.10, while the latter is essentially a High-Pass Filter with a nonuniform stop-band. Frequencies up to 100 Hz are attenuated lightly, higher frequencies below MHz band are attenuated more with peak attenuation around 100 kHz. Frequency response of this filter is given in 4.11.

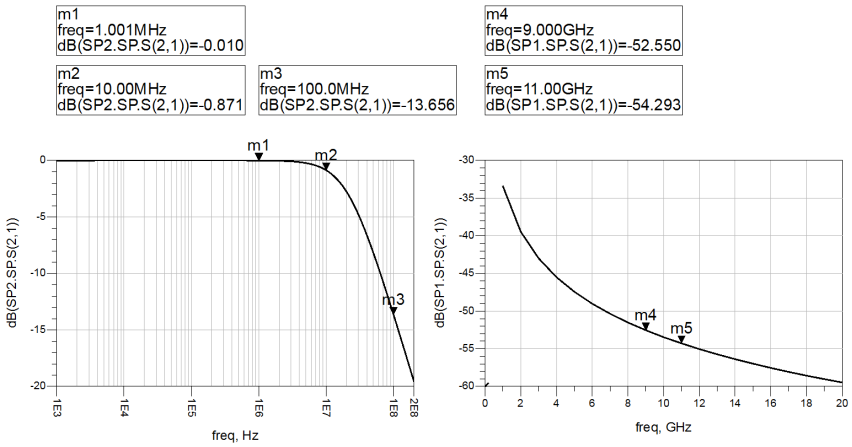

Figure 4.10: Frequency Response of the Feedback Low-Pass Filter

Simulations are done by implementing feedback filters between drain-to-source (DS), drain-to-gate (DG), and source-to-gate (SG) nodes. Each node is either left

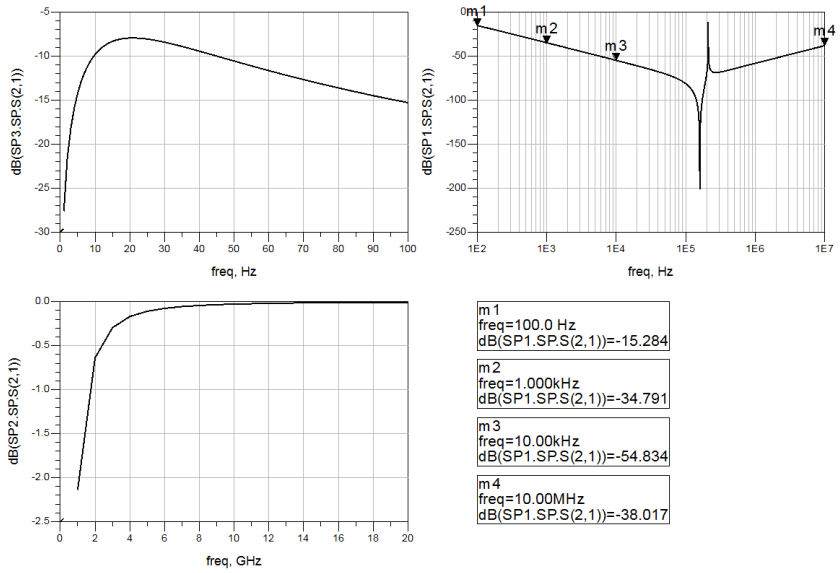

Figure 4.11: Frequency Response of the Feedback Band-Pass Filter

open, or LPF is connected, or BPF is connected. All 27 possible combinations for a single oscillator are simulated. Due to the large number of simulations, a single oscillator is picked for the task.

Combinations are enumerated for the sake of simplicity, and a reference table listing the corresponding feedback filter structures is provided in the Appendix, in Table A.1.

CF4_CG_PB design is simulated at both 9.15 GHz and 11.45 GHz frequencies with varying feedback filters. Simulation results at 9.15 GHz are summarized in Table 4.3. Max. Imp denotes the maximum improvement observed in phase noise with regard to the original oscillator, Freq. denotes the frequency at which the maximum improvement is observed. The last three columns denote the phase noise levels at given offset frequencies.

Simulation results at 11.45 GHz are summarized in Table 4.4.

Low pass filtering reduced the loop gain of low frequencies and hence suppressed the upconversion originated phase noise. This result is consistent with findings reported in the literature.

Table 4.3: Performance Comparison of Feedback Networks at 9.15 GHz

Version	Max. Imp.	Freq.	@100Hz	@1kHz	@10kHz
1	21.1	1	19.4	8.3	1.5
2	34.4	1	23.5	8.1	1.4
3	16.9	4	8.9	-1.2	0.1
4	31.6	1	10.5	-1	0.1
5	30.5	1	22.6	7.33	1.1
6	37.5	1	24.8	8.5	1.5
7	19.4	63.1	18.9	7.9	1.3
8	30.5	1	19.8	7.9	1.3
9	30.9	7.9	23.4	7.6	1.3
10	32.7	12.6	23.8	7.5	1.3
11	28.2	28.2	18.2	7.7	1.3
12	35.7	1	23.8	7.5	1.3
13	23.5	3.1	18.8	7.8	1.3
14	34.0	6.3	23.8	7.5	1.3
15	32.5	1	24.1	7.5	1.3
16	37.5	1	23.9	7.5	1.3
17	37.0	1	24.3	7.5	1.3
18	40.6	1	24	7.5	1.3
19	30.7	1	22.3	7.6	1.3
20	36.7	1	23.9	7.5	1.3
21	26.7	10	22.3	7.7	1.3
22	36.4	1	24	7.5	1.3
23	35.3	6.3	23.9	7.5	1.3
24	40.1	1	24	7.5	1.3
25	34.7	7.9	23.9	7.5	1.3
26	46.0	1	24.1	7.5	1.3

Additional indication of the simulation results is that, incorporation of BPFs provided a better improvement in the phase noise performance, significant in some cases. This improvement could be ascribed to further reduction of the loop gain due to attenuating low frequency bands using BPFs on the feedback path.

The most effective feedback path is drain-to-source connection, which is the output-to-input path for the simulated common gate configuration. However, the improvement provided by implementing additional feedback networks could exceed 10 dB.

Table 4.4: Performance Comparison of Feedback Networks at 11.45 GHz

Version	Max. Imp.	Freq.	@100Hz	@1kHz	@10kHz
1	15.4	1.00	19.40	8.3	1.5
2	27.1	1.00	23.50	8.1	1.5
3	17.2	16.90	8.90	-1.2	0.1
4	28.1	1.00	10.60	-1.0	0.1
5	31.2	1.00	22.60	7.3	1.1
6	39.6	1.00	24.80	8.5	1.5
7	25.3	31.60	24.40	16.6	6.7
8	33.6	33.60	25.40	16.5	6.7
9	32.7	31.60	30.80	16.8	6.7
10	37.0	15.80	32.30	16.7	6.7
11	32.9	20.00	28.80	16.3	6.7
12	40.32	12.60	32.80	16.7	6.7
13	36.7	10.00	26.60	16.5	6.7
14	41.3	8.00	32.60	16.7	6.7
15	32.6	40.00	31.30	16.8	6.7
16	40.5	12.60	33.20	16.7	6.7
17	36.4	25.10	33.00	16.8	6.7
18	42.3	15.90	33.70	16.7	6.7
19	34.0	25.10	30.70	16.7	6.7
20	40.8	12.60	33.10	16.7	6.7
21	37.2	10.00	29.30	16.7	6.7
22	37.5	25.10	33.20	16.70	6.70
23	41.8	8.00	33.00	16.70	6.70
24	42.5	13.00	33.70	16.70	6.70
25	39.7	13.00	33.00	16.70	6.70
26	43.2	10.00	33.60	16.70	6.70

Versions with BPF in drain-to-gate connection have slightly worse performance than their counterparts.

Results of given simulations do not cover the filtering of loop 4 shown in Fig.4.9. In order to investigate a possible effect, resonator coupling arm is DC blocked and bias resistor and voltage values are set accordingly to keep the same operating point. Therefore the loop for near-DC frequencies is reduced more.

Results are summarized in Table 4.5.

Phase noise performance results of DC blocking the resonator are given in

Table 4.5: Performance Comparison of Feedback Networks at 11.45 GHz when DR is DC blocked

Version	Max. Imp.	Freq.	@100Hz	@1kHz	@10kHz
1	15.6	63.1	15.3	5.0	0.4
2	26.0	20	20.2	4.6	0.3
3	2.8	50.1	2.2	-0.3	-0.1
4	8.1	15.8	2	-0.4	-0.1
5	20.0	39.8	18.6	4.8	0.2
6	28.5	20	21.7	5	0.3
7	15.3	63.1	15.1	5.1	0.2
8	16.3	31.6	15.6	5	0.2
9	24.6	25.1	20	4.7	0.2
10	25.9	25.1	20.9	4.6	0.2
11	19.8	31.6	17.1	4.9	0.2
12	27.9	20	21.1	4.6	0.2
13	19.2	15.8	15.7	5	0.2
14	27.5	15.8	21	4.6	0.2
15	22.7	39.8	20.9	4.6	0.2
16	28.8	20	21.3	4.6	0.2
17	27.5	20	21.4	4.6	0.2
18	31.1	15.8	21.4	4.5	0.2
19	22.6	31.6	20	4.7	0.2
20	28.7	20	21.2	4.7	0.2
21	22.1	20	19.1	4.7	0.2
22	27.7	20	21.3	4.6	0.2
23	28.5	15.8	21.2	4.6	0.2
24	31.1	15.8	21.4	4.5	0.2
25	28.0	20	21.2	4.6	0.2
26	31.0	12.6	21.4	4.5	0.2

Fig.4.12 and Fig.4.13.

Improvement in close-in phase noise is observed in both cases. This result is consistent with the low frequency loop approach adopted, since DC blocking the resonator without altering the device operating point is effectively filtering low frequency components in loop 4, as illustrated in Fig.4.9

Also a residual phase noise improvement around 6 dB is observed at 9.15 GHz.

In order to investigate the effect of attenuation amount of the low frequencies,

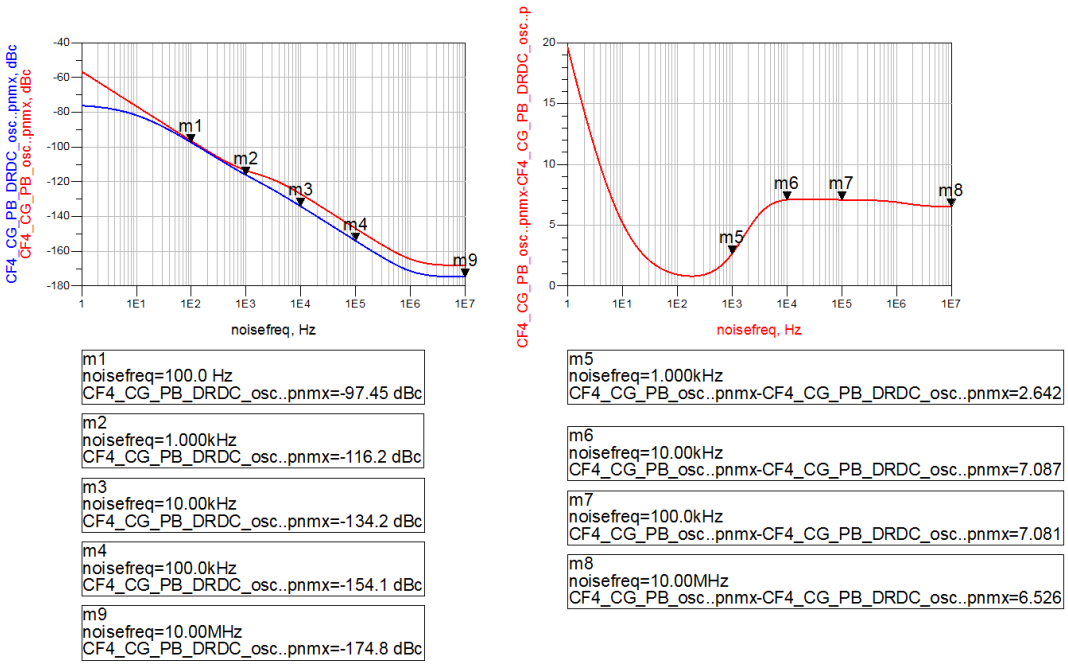

Figure 4.12: Effect of DC blocking the resonator at 9.15 GHz

HPFs that eliminate the band completely are utilized in some of the configurations but they did not operate as effective as implemented networks. Although not simulated equally extensively, the maximum phase noise improvement did not exceed 30 dB, which is 10 dB lower than the maximum suppression achieved by implemented feedback networks.

Phase noise spectra for the ultimate improvements obtained at 9.15 GHz and 11.45 GHz oscillation frequencies by implementing low frequency feedback and large signal analysis methods are given in Fig.4.14 and Fig.4.15, respectively.

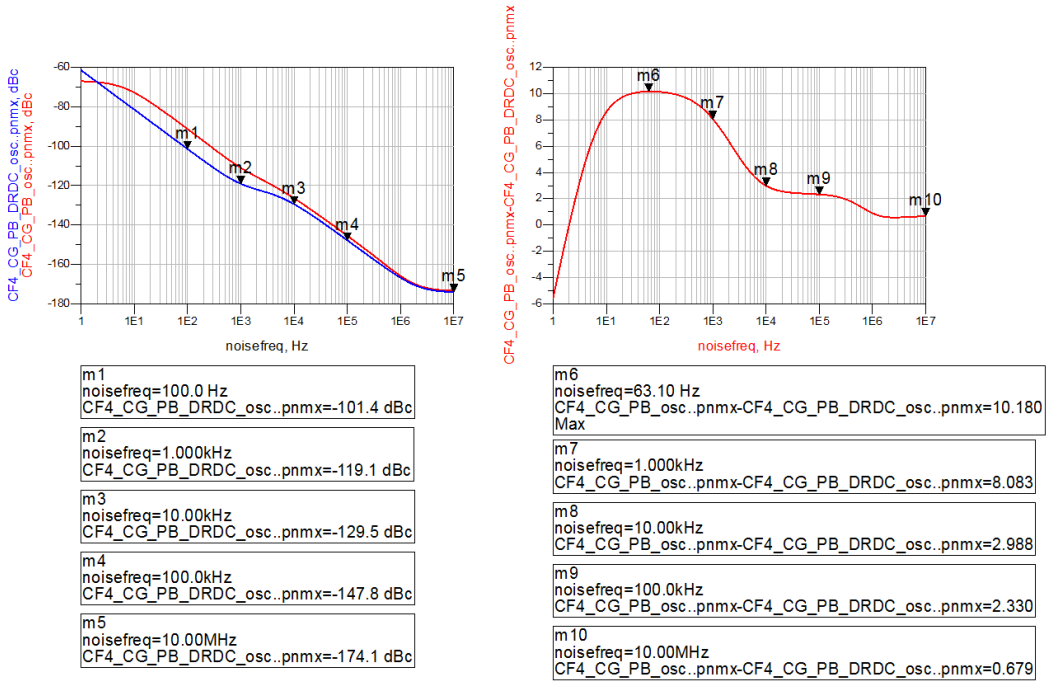

Figure 4.13: Effect of DC blocking the resonator at 11.45 GHz

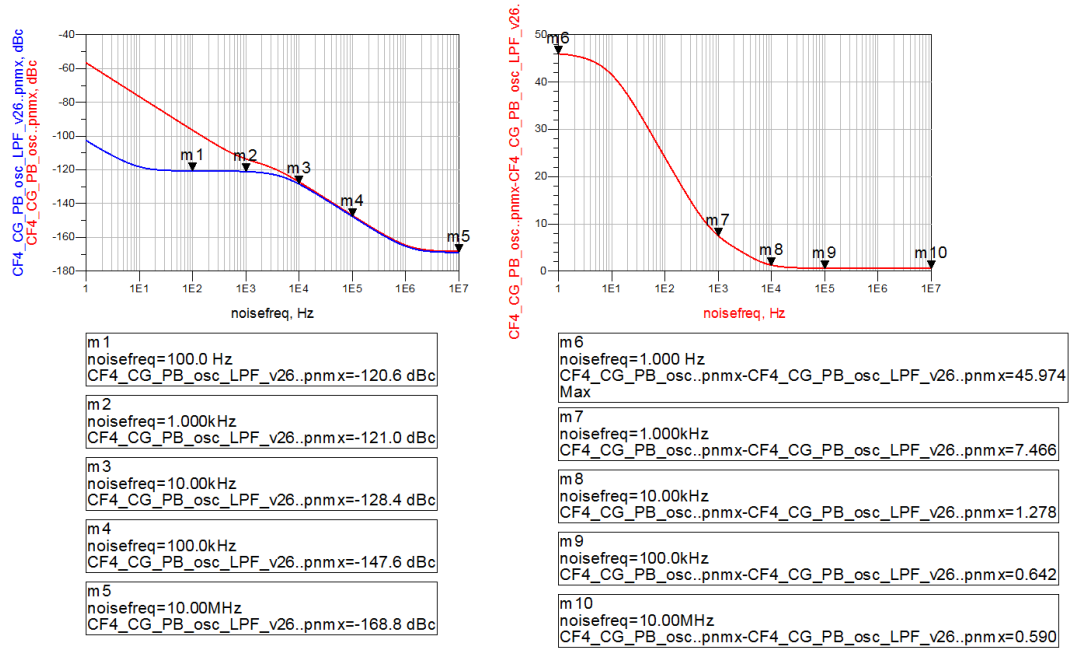

Figure 4.14: Maximum Phase Noise Improvement at 9.15 GHz

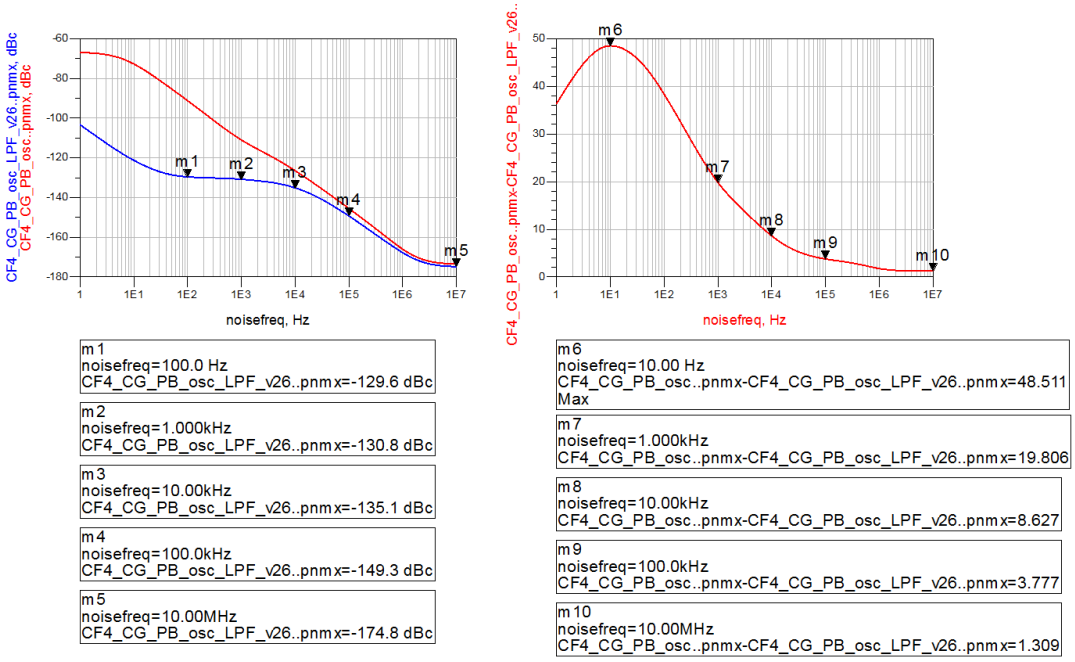

Figure 4.15: Maximum Phase Noise Improvement at 11.45 GHz

Chapter 5

Conclusion

A DRO design is presented using nonlinear device models and resonator measurements. Extensive simulations are done in order to understand the configuration, circuit and parameter dependencies of phase noise performance.

Large signal analysis method that defines an optimum at an abstraction level is realized within an RF and Electromagnetic co-simulation environment, and parameter dependencies are illustrated. Frequency response of two dielectric resonators with different resonant frequencies are measured by using a microstrip coupling test fixture. Measurement results are shown to be in agreement with the ideal resonator models. Measured data is imported into the RF/EM co-simulation environment and used as input to Harmonic Balance simulation of the oscillator. Resonator coupling parameters are shown to be significant on phase noise performance of the oscillator. Simulation results of oscillator circuits both with ideal resonator models and imported measurement data are shown to be consistent with optimum coupling parameters suggested in the literature.

Simulation structure for testing and implementing the optimum phase noise performance condition defined in Kurokawa model is proposed and explained. Using these simulation steps; phase noise is shown to be suppressed up to 20 dB at 100 kHz offset, at 9.15 GHz. Suboptimal designs are compared with the best case

in terms of Kurokawa condition, and they are shown to have varying characteristics while being indifferent to Nyquist criterion. Therefore it was demonstrated by simulation that the proposed design method contributes to improve the design of oscillator circuits.

Low frequency feedback technique which constitutes a significant improvement method in phase noise reduction is implemented and tried. Improvements in close-in phase noise performance are observed in simulation results. The essential low frequency feedback method that is reported in the literature is adding low pass filter, which essentially stabilizes -or limits- the low-frequency gain, between output and input ports of the circuit. This simple procedure is implemented and results are reported. In addition to this method, further filtering is implemented and simulated between all three ports of the transistor in order to investigate the suppression effect on the nonlinear capacitances of the transistor. Results suggest that additional filtering improves the phase noise performance further, around 10 dB.

Although a generalized method that is reproducible for every device or process is still not available, the methods presented cover the evaluation of design steps that are needed to be checked in order to obtain low phase noise. It can be concluded that, designing a low phase noise oscillator is a process that heavily depends on the careful analysis of the characteristics of used active device.

It is believed that use of a load pull device or similar equipment for the purpose of accurately characterizing and setting as required the input impedance of the transistor would be greatly beneficial, since the performance of the circuit is highly dependent on proper input and output matching.

Also it should be noted that the use of layout components that are EM simulated in Agilent Momentum, gives different phase noise results than using microstrip components in Agilent ADS that have identical frequency responses, up to 8 dB. A possible reason for such behavior is the undefined near DC behavior of RF simulation components. Therefore apart from the accuracy concerns, EM components should be used in EM/Co-circuit simulations in order to accurately analyze low frequency behavior of the whole circuit.

The method for designing an oscillator with low phase noise both close and away from the carrier is developed and presented. By implementing low frequency networks, significant improvement is observed in close-in frequencies. Combined with the optimization for Kurokawa condition, better residual phase noise performance is obtained in whole spectrum of phase noise, as high as 45 dB, both at 9.15 GHz and 11.45 GHz.

Effects of the parameters of implemented low frequency feedback networks on phase noise performance could be further investigated in the future.

Bibliography

[1] R. P. J. Graffeuil, "Low frequency noise properties of microwave transistors and their application to circuit design," *24th European Microwave Conference*, vol. 1, pp. 62–75, 1994.

[2] E. Rubiola, *Phase Noise and Frequency Stability in Oscillators*. Cambridge, UK: Cambridge University Press, 2009.

[3] J. Johnson, "The schottky effect in low frequency circuits," *Physical Review*, vol. 26, no. 1, pp. 71–85, 1925.

[4] M. Planat, *Noise, Oscillator and Algebraic Randomness From Noise in Communications to Number Theory*. Berlin Heidelberg: Springer-Verlag, 1999.

[5] S. Watanabe, "Multi-lorentzian model and 1/f noise spectra," *Journal of the Korean Physical Society*, vol. 3, pp. 646–650, 2005.

[6] Y. J. P. Sung-Min Hong, Chan Hyeong Park and H. S. Min, "Physics-based analysis and simulation of 1/f noise in mosfets under large-signal operation," *IEEE Transactions on Electron Devices*, vol. 57, pp. 1110 – 1118, 2010.

[7] C. F. Pier Andrea Traverso, "An empirical bipolar device nonlinear noise modeling approach for large-signal microwave circuit analysis," *IEEE Transactions on Microwave Theory and Techniques*, vol. 54, no. 12, pp. 4341–4352, 2006.

[8] E. S. Ferre-Pikal and F. H. Savage, "Up-converted 1/f pm and am noise in linear hbt ampliers," *IEEE Transactions on Ultrasonics, Ferroelectrics, and Frequency Control*, vol. 55, no. 8, pp. 1698–1704, 2008.

[9] T. H. Morshed and M. V. Dunga, "Compact modeling of flicker noise variability in small size mosfets," *Electron Devices Meeting (IEDM), 2009 IEEE International*, pp. 1–4, 2009.

[10] K. S. Svetlana A. Vitusevich, "Design and characterization of an all-cryogenic low phase-noise sapphire k-band oscillator for satellite communication," *IEEE Transactions on Microwave Theory and Techniques*, vol. 51, no. 1, pp. 163–169, 2003.

[11] A. K. P. Ulrich L. Rohde and G. Boeck, *The Design of Modern Microwave Oscillator for Wireless Applications*. Hoboken, New Jersey: John Wiley & Sons, 2005.

[12] R. W. Rhea, *Discrete Oscillator Design Linear, Nonlinear, Transient, and Noise Domains*. Norwood, MA: Artech House, 2010.

[13] C. B. J.K.A. Everard, "Reduced transposed flicker noise in microwave oscillators using gaas-based feedforward amplifiers," *IEEE Transactions on Ultrasonics, Ferroelectrics and Frequency Control*, vol. 54, no. 6, pp. 1108 – 1117, 2007.

[14] R. G. Rogers, *Low Phase Noise Microwave Oscillator Design*. Norwood, MA: Artech House, 1991.

[15] R. W. Rhea. personal communication.

[16] A. K. P. Ulrich L. Rohde, "Tunable active inductor offers integrable and cost-effective alternatives of varactor tuned vcos," *Frequency Control Symposium, 2009 Joint with the 22nd European Frequency and Time forum. IEEE International*, pp. 962–967, 2009.

[17] A. A. A. Emad Hegazi, "Varactor characteristics, oscillator tuning curves, and amfm conversion," *IEEE Journal of Solid-State Circuits*, vol. 38, no. 6, pp. 1033–1039, 2003.

[18] J. N. A. Victor, "Noise characteristics of an oscillator with a barium strontium titanate (bst) varactor," *IEE Proceedings on Microwaves, Antennas and Propagation*, vol. 153, no. 1, pp. 96–102, 2006.

[19] D. Leeson, "A simple model of feedback oscillator noise spectrum," *Proceedings of the IEEE*, vol. 54, pp. 329–330, 1966.

[20] G. Gonzalez, *Foundations of Oscillator Circuit Design*. Norwood, MA: Artech House, 2007.

[21] W. Robins, *Phase Noise in Signal Sources*. Herts, UK: The Institution of Engineering and Technology, 1982.

[22] T. L. A. Hajimiri, "A general theory of phase noise in electrical oscillators," *IEEE Journal of Solid-State Circuits*, vol. 33, no. 2, pp. 179–194, 1998.

[23] J. Everard, *Fundamentals of RF Circuit Design with Low Noise Oscillators*. Hoboken, New Jersey: John Wiley & Sons, 2001.

[24] A. Grebennikov, *RF and Microwave Transistor Oscillator Design*. Hoboken, New Jersey: John Wiley & Sons, 2007.

[25] K. Kurokawa, "Some basic characteristics of broadband negative resistance oscillator circuits," *Bell System Technical Journal*, vol. 48, no. 6, pp. 1937–1955, 1969.

[26] J. Piekarski and K. Czuba, "The method of designing ultra low phase noise dielectric resonator oscillators," *18th International Conference on Microwave Radar and Wireless Communications (MIKON)*, pp. 1–4, 2010.

[27] C.-Y. S. Hans Rohdin and C. Stolte, "A study of the relation between device low-frequency noise and oscillator phase noise for gaas mesfets," *Microwave Symposium Digest, 1984 IEEE MTT-S International*, pp. 267–269, 1984.

[28] M. Golio and J. Golio, *RF and Microwave Passive and Active Technologies*. Boca Raton, FL: CRC Press, 2008.

[29] D. Kajfez and P. Guillon, *Dielectric Resonators*. Norwood, MA: Artech House, 1986.

[30] R. D. Richtmyer, "Dielectric resonators," *Journal of Applied Physics*, vol. 10, no. 6, pp. 391–398, 1939.

[31] M. T. Sebastian, *Dielectric Materials for Wireless Communication*. Amsterdam, Netherlands: Elsevier BV, 2008.

[32] K. Y. Mark M. Nelson and M. Thomason, "Efficacy of fluorine doping at various stages on noise reduction," *2005 IEEE Workshop on Microelectronics and Electron Devices*, pp. 17–20, 2005.

[33] E. N. Ivanov and M. E. Tobar, "Low phase-noise sapphire crystal microwave oscillators: current status," *IEEE Transactions on Ultrasonics, Ferroelectrics, and Frequency Control*, pp. 263–269, 2009.

[34] I. Ibrahim and H. Heuermann, "Improvements in the flicker noise reduction technique for osillator designs," *European Microwave Conference 2009*, pp. 1215 – 1218, 2009.

[35] J. J. Majewski, "New method of phase noise and intermodulation distortion reduction in high-order qam systems," *13th International Conference on Microwaves, Radar and Wireless Communications MIKON-2000*, vol. 1, pp. 258–264, 2000.

[36] M. Prigent and J. Obregon, "Phase noise reduction in fet oscillators by low-frequency loading and feedback circuitry optimization," *IEEE Transactions on Microwave Theory and Techniques*, vol. 35, no. 3, pp. 349–352, 1987.

[37] C. Sanabria, *Noise of AlGaN/GaN HEMTs and Oscillators*. PhD thesis, University of California Santa Barbara, 2006.

[38] A. M. P. George D. Vendelin and U. L. Rohde, *Microwave Circuit Design Using Linear and Nonlinear Techniques*. Hoboken, New Jersey: John Wiley & Sons, 2005.

[39] F. Kusidlo. personal communication.

[40] J. Gao and G. Boeck, "Relationships between common source, common gate, and common drain fets," *IEEE Transactions on Microwave Theory and Techniques*, vol. 53, no. 12, pp. 3825–3831, 2005.

[41] "Design considerations for a ku-band dro in digital communication systems," Tech. Rep. AN1035, California Eastern Laboratories, April 2003.

[42] M. X. Jeremy Everard and S. Bale, "Simplified phase noise model for negative-resistance oscillators and a comparison with feedback oscillator models," *IEEE Transactions on Ultrasonics, Ferroelectrics, and Frequency Control*, vol. 59, no. 3, pp. 382–390, 2012.

Appendix A

Feedback Configurations

Feedback networks implemented in circuits are defined in Table A.1. L and B stand for LPF and BPF, respectively.

Table A.1: Feedback Networks Implemented

Version	DS	DG	SG
1	-	-	L
2	-	-	B
3	-	L	-
4	-	B	-
5	L	-	-
6	B	-	-
7	-	L	L
8	-	B	L
9	-	L	B
10	-	B	B
11	L	L	-
12	B	L	-
13	L	B	-
14	B	B	-
15	L	-	L
16	B	-	L
17	L	-	B
18	B	-	B
19	L	L	L
20	B	L	L
21	L	B	L
22	L	L	B
23	B	B	L
24	B	L	B
25	L	B	B
26	B	B	B